Probing Water Properties and Cationic Exchange in Calcium-Silicate-Hydrate

An Atomistic Modeling Study

by

Mostafa Youssef Mahmoud Youssef

B.S., Nuclear Engineering (2006)

Alexandria University

Submitted to the Department of Nuclear Science and Engineering

in partial fulfillment of the requirements for the degree of

Master of Science in Nuclear Science and Engineering

at the

MASSACUSETTS INSTITUTE OF TECHNOLOGY

June 2010

Signature of Author: _____

Department of Nuclear Science and Engineering

May 21, 2010

Certified by: _____

Bilge Yildiz

Assistant Professor of Nuclear Science and Engineering

Thesis Supervisor

Certified by: _____

Roland Pellenq

Visiting Professor of Civil and Environmental Engineering

Thesis Reader

Certified by: _____

Sidney Yip

Professor of Nuclear Science and Engineering, and Materials Science and Engineering

Thesis Reader

Accepted by: _____

Jacquelyn C. Yanch

Professor of Nuclear Science and Engineering

Chair, Department Committee on Graduate Students

Probing Water Properties and Cationic Exchange in Calcium-Silicate-Hydrate

An Atomistic Modeling Study

by

Mostafa Youssef Mahmoud Youssef

Submitted to the Department of Nuclear Science and Engineering on May 21, 2010 in partial fulfillment of the requirements for the Degree of Master of Science in Nuclear Science and Engineering

Abstract

Two problems related to the assessment of the performance of cementitious materials in the nuclear fuel cycle are investigated by means of atomistic simulations. The first is the structural and dynamic nature of water confined in the nano-pores of the highly disordered calcium-silicate-hydrate (C-S-H) which is the major binding phase of cement. The microscopic structure and dynamics of water confined in C-S-H have important implications on describing the cohesion and mechanical behavior of cement from its setting to its aging; nevertheless they have not been fully elucidated prior to this thesis. The second problem is the encapsulation of strontium-90, an important radionuclide, in C-S-H and its crystalline analogue tobermorite 9 Å by means of cationic exchange with calcium.

We showed that the nature of the interaction between the confined water and C-S-H is hydrophilic. The interlayer calcium ions and the disorder in the silicate chains act synergistically to achieve this hydrophilic interaction. The water molecules ultra-confined in this hydrophilic and disordered interlayer space adopt a unique multi-range structure: at short range they are tetrahedrally coordinated but with distortions, at intermediate range they exhibit a structure similar to that of dense fluids and supercooled phases, and at ranges up to 10 Å spatial correlations persist through dipole-dipole interactions that are enhanced by the directionality of the hydrogen bonds formed between the confined water and the defective silicate chains. This confined water exhibits a three-stage dynamics evidenced in the mean square displacement (MSD) results, with a clear cage stage characteristic of glassy dynamics similar to that of supercooled liquids and glass forming materials. The glassy dynamics is induced primarily because of the attractive interactions of water molecules with the calcium silicate walls, serving to constrain the motion of the water molecules at the interface, as if with an effective temperature lower than the actual simulation temperature. At intermediate time scales that correspond to the β-relaxation of glassy materials, the non-Gaussian parameter indicates a significant heterogeneity in the translational dynamics of the confined water, also consistent with the cage stage identified in the MSD of the water molecules.

Strontium was shown to favor energetically substituting calcium in the interlayer sites in C-S-H and tobermorite 9 Å with the trend more pronounced in the latter. The silicate chains in both cementitious waste forms were not affected by strontium substitution within our molecular dynamics simulation. Finally, we observed degradation in the mechanical properties in the strontium-containing cementitious waste form. The

degradation increases with the increase of strontium concentration, but overall this degradation is not limiting for the use of C-S-H or tobermorite 9 Å as candidates in immobilizing radioactive strontium.

Thesis Supervisor: Bilge Yildiz

Title: Assistant Professor of Nuclear Science and Engineering

Acknowledgements

I would like to express my deepest gratitude to professor Bilge Yildiz, my thesis supervisor, for her help, guidance and support throughout this work. Our thoughtful discussions were always stimulating to achieve the goals. Working in her research group was very enriching to my knowledge and research experience. Her kindness, patience and understanding made it possible to overcome all the hardships while finishing this work.

I would like to gratefully acknowledge professor Sidney Yip and professor Roland Pellenq, my thesis readers, for very helpful conversations and comments. It was very beneficial for me to interact and learn from you. Your encouragement and support is very much appreciated.

I owe special thanks to Dr. Akihiro Kushima whose unconditional help and kindness made my first steps in learning computer simulation of materials much easier. In addition, I also thank all the members of the Concrete Sustainability Hub (CSH) at MIT for helpful discussions.

Very special thanks to my home university, Alexandria University, in Egypt where I acquired the basis of my knowledge as an undergraduate student. In particular, I would like to thank professor Alya Badawi, professor Mohamed El-Affify and professor Hanaa Abou Gabal. In addition, I would like to thank a very great mentor and friend from Alexandria University, professor Amr Mohamed. I'm deeply indebted to you for all the help, advice and friendship.

I also thank my great friends, Mostafa Mahmoud, Abdel Rahman Hassan, Ahmed Hamed and Khabiboulakh Katsiev. I am so lucky to have amazing friends like you.

There are no words can describe my gratitude to my dearest, closest and most important people in my life, my mother and my sister. There is no moment passed in my life without me feeling your endless love and care. There is no success I accomplished without you supporting me. To you I dedicate this thesis.

Table of Contents

List of Figures

List of Tables

Chapter 1: Introduction, Background and Objective

1.1 Introduction

Cement-based materials in general and concrete in particular are used in the construction of various nuclear facilities because of three major reasons. First, these materials are known for their structural strength and durability over very long periods of times. Second, they are able to shield effectively against radiation and against the migration of radionuclides. Third, a great experience in producing these materials at very low cost compared to other structural materials was accumulated over thousands of years.

At every stage of the nuclear fuel cycle, cement-based materials play a major role in providing support, shielding and containment. For example, concrete structures are used as storage pool for the fresh nuclear fuel. Later on when the nuclear fuel is in operation in the nuclear power plant, the concrete containment* is the outermost barrier that shields against any leakage of radioactivity to the biosphere and is also known to be the only irreplaceable component of the nuclear power plant. Furthermore, concrete structures serve as an interim for the spent nuclear for decades after the operation in the nuclear power plants. Finally, cementitious materials can be used as the waste form[12] and/or a container[11] for the whole waste package for the ultimate disposal of radioactive materials in geological repositories.

Understanding on a fundamental level the long-term performance of cement-based materials and developing capabilities to project their lifetimes is of utmost

* Out of 104 commercial nuclear power plant in the US, 34 employed reinforced concrete containment and 37 employed post-tensioned concrete containement.[1]

importance. To that end we believe that computational science techniques exemplified by atomistic simulation is able to provide such a fundamental understanding and can be utilized as a predictive tool as well. Historically atomistic simulation techniques were not used in concrete/cement science because of the complexity involved in modeling these materials. However, with the recent advances in our understanding of the structure of cementitious materials at the nanoscale[213] and the atomic scale,[3] it is possible now to incorporate atomistic simulation techniques in studying cementitious materials on equal footing with experimental techniques.

In this thesis we consider two problems relevant to assessing the performance of cementitious materials by means of atomistic simulation. The first, is understanding the structure and dynamics of the water confined in the smallest pores (< 1nm) of calcium-silicate-hydrate which is the major binding phase that controls the chemistry and mechanics of cement. This is regarded as the first step to informing the dependencies of the cement paste cohesion and mechanics on this ultra-confined water structure and dynamics. The second problem is exploring the stability of cementitious materials upon cationic exchange between the host cations and the radionculides to be disposed. The mechanical integrity of the cement/radionuclide waste form system is also investigated to assess its ability to prevent the release of radionuclides into the environment.

In the rest of this chapter we briefly review the components and structure of concrete and cement, and finally we conclude by a statement of the objective of this thesis.

1.2 Concrete, Cement and Calcium-Silicate-Hydrate

Concrete is the major form of cementitious materials. It is a low cost and low energy material made from the most available elements on earth. Every year more than 1 m^3 is produced per person worldwide[4]. There are three basic ingredients in the concrete mix:

1- Cement: When cement is mixed with water it forms a paste that hardens and binds the aggregates together.

2- Water: Water is needed to react chemically with cement. The amount of water to cement (w/c ratio) is an important controlling factor of concrete strength because of the clinker phase dissolution kinetics that depends on water content. In general the lower w/c, the stronger the concrete is because of a denser final structure. However, enough water must be added to make the mix workable.

3- Aggregates: Aggregates are usually sand and crushed stones are used in most mixes.

The hardened cement paste is the only continuous phase in concrete and all transport processes depends primarily on the structure of this paste.[5,6] The most common type of cement that is used by concrete manufacturers is Portland cement which is prepared by grinding, blending and firing of raw materials composed mainly of calcium carbonates and aluminum silicates. Then to produce a hardened product, water must be mixed with cement. Upon this mixing a wide range of chemical reactions take place and they are generally referred to by the term hydration. These reactions have diverse rates and some of them continue to take place even after installing the paste in the actual construction. So the outcome of the hydration process are solid phases, those who already

reacted with water and others that did not react yet, cross linked by a three dimensional network of pores filled with water. The major reacted solid products are:

1- Calcium-Silicate-Hydrate gel (C-S-H): It is a poorly crystalline product of variable composition and has a layered structure similar to that of the mineral analogue tobermorite. It makes up about one-half to two-thirds of the volume of the hydrated paste and it controls the chemical and mechanical behavior of the paste.

2- Calcium Hydroxide ($Ca(OH)_2$): A crystalline material that occupies about 20-25 % of the paste volume.

3-Aluminoferrite trisulphate (Ettringite or AFt).

On the other hand, the three dimensional network of pores is filled with water with high alkalinity pH >11 which varies depending on the type of cement. These pores can be interconnected or isolated and they are usually classified according to size into three categories:[7]

1- Nano-pores: These are also referred to as interlayer pores as they separate the layers of the single C-S-H particle. Their size is less than 1 nm.

2- The C-S-H gel pores: These are on the order of the size of the elementary C-S-H particle ~ 5 nm and they separate the C-S-H particles, while still retaining the cohesion of the cement paste.

3- The capillary pores: They have a characteristic size of tens to hundreds of nanometers.

This summary shows that the hardened cement paste is a very complex system with different phases, interfaces and continuously ongoing chemical reactions. However, since the C-S-H makes up the bulk of the paste matrix, it is reasonable to assume that it dominantly controls the paste properties. This is indeed true[568] and it is very common in cement and concrete science to explain many of concrete and cement properties in terms of C-S-H chemistry.

C-S-H is a nonstoichiometric poorly-crystallized compound. The basic unit of C-S-H is small particles that have a characteristic length of 5 nm. Figure 1.1 shows a schematic diagram of these particles which have an internal sheet like structure similar to that of the minerals tobermorite and jennite with a layer thickness in the sub-nanometer range. It is accepted that the two-dimensional backbone of a C-S-H layer is a double plane of Ca^{2+} ions 6 or 7-coordinated by central O^{-2} ions, to which disordered finite length silicate chains are grafted on each side.[9] The interlayer space contains trapped water molecules and interlayer calcium ions.

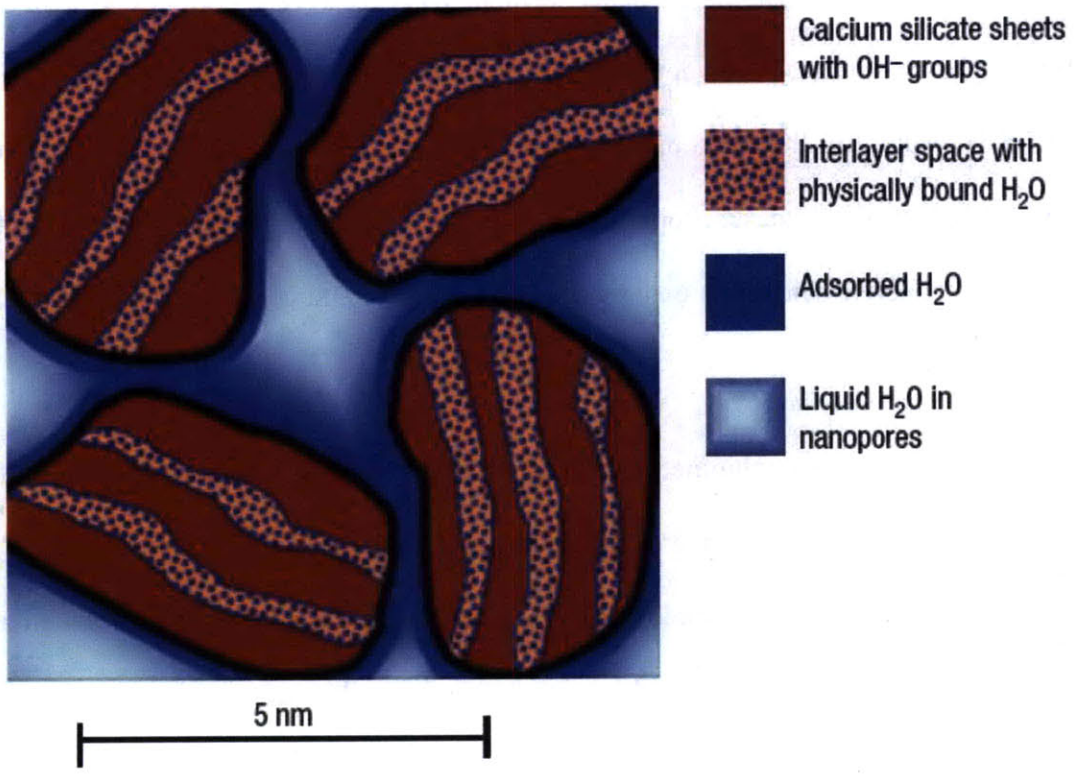

Figure 1.1 Schematic diagram of the nano-scale C-S-H particles, depicted by Allen et al. in reference 2

Although the structure of C-S-H is highly disordered and thus imposes a great difficulty in modeling, there are certain well-known facts about that were used as constraints to design the model that we adopt in this thesis. These facts are:

1- C-S-H is usually characterized by calcium to silicon ratio (C/S) in its particles. This ratio varies from paste to paste and even varies spatially within the single paste. However, it is generally accepted that the average value of this ratio in cement is 1.7. [2,9]

2- The density of a C-S-H particle whose C/S =1.7 was accurately determined by small angle neutron scattering measurements and was found to be 2.604 g/cm^3.[2]

3- The building block of the finite length silicate chains is the silicate tetrahedron denoted by Q^n where $0 \leq n \leq 4$. Here n is the number of oxygen ions that bridge to adjacent tetrahedra; thus Q^0 are isolated tetrahedra, Q^1 are chain-end groups, Q^2 middle groups, Q^3 and Q^4 lead to complicated three dimensional structures.[10] Nuclear Magnetic Resonance experiments[3] showed that C-S-H in cement pastes with C/S =1.7 has Q^0 at ~10 %, Q^1 at ~ 67% and Q^2 at ~ 23%, and does not have Q^3 or Q^4.3

By applying the first and third facts as constraints, Pellenq et al. were able to construct a successful model for two sheets of a C-S-H particle separated by interlayer water and calcium ions.[3] This model successfully accounts for many structural (radial distribution functions), mechanical (elastic constants) and chemical (Infra Red spectra) properties without being fitted to reproduce any of them. In Figure 1.2, we show the atomistic structure of this model. The model consists of two layers of calcium (sky blue) oxide (red). Finite length silicate chains (silicon is green) are also shown grafted on the layers. In addition, water molecules (red oxygen and white hydrogen) are trapped in the interlayer space and also trapped in small cavities within the calcium-silicate layers. Interlayer calcium (yellow) coexists with water in the interlayer space. For this model C/S is 1.65 and the final density is 2.56 g/cm^3. By introducing this C-S-H model as the starting point in representing the cementetious materials in this thesis, we can now turn into formulating the objective of this thesis.

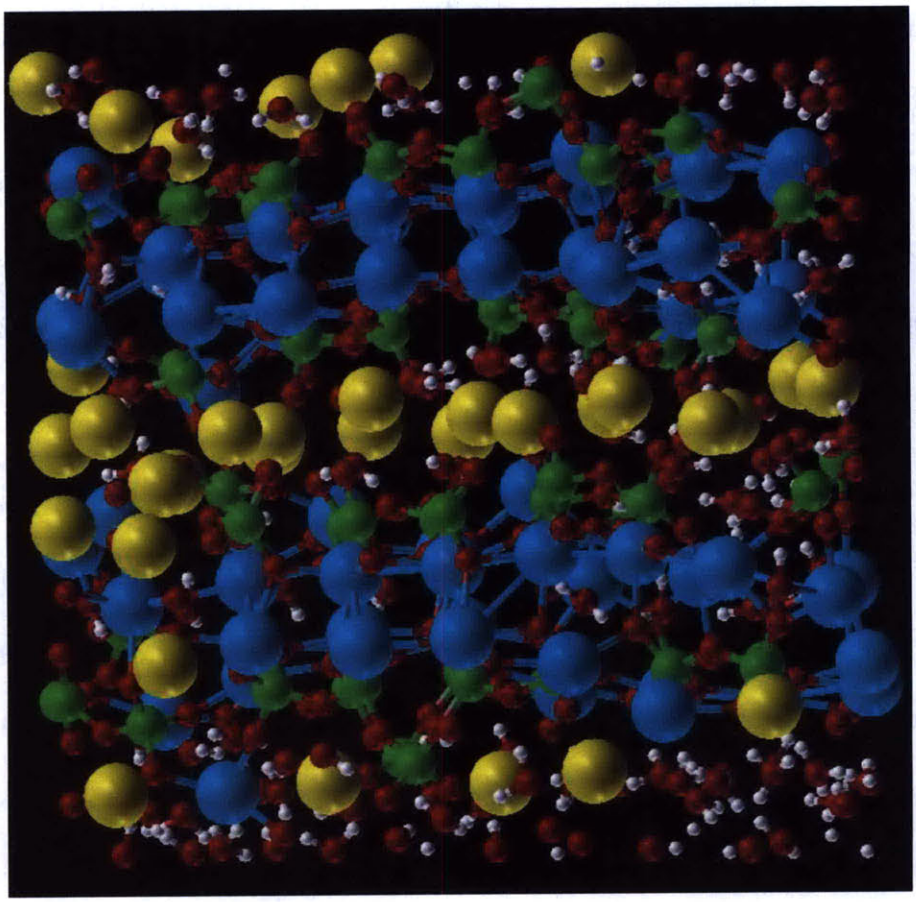

Figure 1.2 Schematic of the recently developed atomistic model of C-S-H.[3] It consists of two highly disordered layers of calcium-silicate and water molecules trapped in the interlayer space together with interlayer calcium ions. Few water molecules are trapped in small cavities in the calcium-silicate layers. White spheres are hydrogen atoms, red are oxygen, green are silicon, light blue are layer calcium and yellow are interlayer calcium.

1.3 Thesis Objective and Organization

Our objective in this thesis is twofold. First is elucidating the nature of the water confined in the geometrically and chemically heterogeneous interlayer space of the C-S-H particle using atomistic simulation techniques. This part of the thesis will focus on the structure, dynamics, polarization and hydrogen bonding of this ultra-confined water and will be covered in the second chapter of the thesis. This fundamental study of the

confined water in C-S-H is regarded as the first step in delineating the inter-relationships between the cement paste cohesion and the mechanical and chemical properties of this type of water. It also serves to separate the role of this ultra-confined water in the cement paste from the role of the other types of water that are confined at larger length scales (see section 1.2). Furthermore, this study has a direct impact in understanding aging phenomena in the irreplaceable concrete containment in nuclear power plants. A major aging mechanism in these structures is the loss of water due to the long-term exposure to elevated temperature and to direct heating by radiation, rendering mechanical properties of concrete become unfavorable.

The second objective is understanding the effect of the cationic exchange between the calcium cation (Ca^{2+}) in cement and the radionuclide strontium-90 ($^{90}Sr^{2+}$) on the stability and mechanical integrity of a cementitiuos waste form. This radionuclide ($^{90}Sr^{2+}$) is a fission product that contributes significantly to the bulk radioactivity and decay heat in the spent nuclear fuel for several decades after the discharge from the nuclear power plant. Thus, it is essential to assess the performance of a cementitious waste form in encapsulating this radionuclide. Our tools in this assessment is atomistic simulation techniques as well. This problem will be treated in the third chapter of the thesis.

Finally, the fourth chapter is an epilogue for the thesis and an outlook for future work. Several computational details are collected in appendices at the end of the thesis. These are important in reproducing this work in the future by other interested researchers.

1.4 References

1. Naus, D. J. *Primer on Durability of Nuclear Power Plant Reinforced Concrete Structurues- A review of Pertient Factors*, NUREG/CR-6927, 2007.
2. Allen, A.; Thomas, J.; Jennings, H. *Nature Materials* 2007, *6*, 311.
3. Pellenq, R.; Kushima, A.; Shahsavari, R.; Van Vliet, K.; Buehler, M.; Yip, S.; Ulm, F.-J. *Proc. Natl. Acad. Sci. U.S.A.* 2009, *106*, 16102.
4. Scrivener, K. L.; Kirkpatrick, R. J. *Cement and Concrete Research* 2008, *38*, 128.
5. Mindess, S.; Young, J. F. *Concrete*, Prentice Hall: Englewood Cliffs, NJ, 1981.
6. Neville A. M. *Properties of Concrete*, 4th ed.; Prentice Hall: Upper Saddle River, NJ, 1995.
7. DeJong; J.; Ulm, F.-J. *Cem. Concr. Res.* **2007**, *37*, 1.
8. Taylor, H. F. W. *Cement Chemistry*, 2nd ed.; Thomas Telford: London, 1997.
9. Pellenq, R. J. –M.; Van Damme, H. *MRS Bulletin* May 2004, 319.
10. I. G. Richardson, *Cem. Concr. Res.* **2004**, *34*, 173.
11. Forsberg, C. W.; Dole, L. *International High-Level Radioactive Waste Management Conference,* Las Vegas, 2008.
12. Wiedland, E.; Johnson, C. A.; Lothenbach, B.; Winnefeld, F. *Mat. Res. Soc. Symp. Proc.* 2006, *932*.
13. Skinner, L. B.; Chae, S. R.; Benmore, C. J.; Wenk, H. R.; Monteiro, P. J. M. *Phys. Rev. Lett.* **2010**, *104*, 195502.

Chapter 2: The Nature of Ultra-Confined Water in C-S-H

2.1. Introduction

Water is the most abundant compound on the surface of the Earth and it is the principal constituent of all living organisms.[1] Very often water is found in confined geometries. Confined water at the nanometer scale differs significantly from bulk water. For example, by confining water in nano-pores, so narrow that the liquid cannot freeze, it is possible to explore its properties well below its homogeneous nucleation temperature.[6,7] Widespread interest exists in the structure and dynamics of water in confinement, and the influence of confinement on the hydrogen bonding, interfacial transport, and mechanics.[66,67] In the very fundamental biological system, the cell, water is confined between crowded bimolecular assemblies that are separated by 2-3 water layers.[2] Other systems of importance and to which water confinement is relevant are layered clays[3], zeolites[4], and cement.[5]

In spite of this interest in understanding confined water properties, our knowledge in this area is still developing. While there is sufficient evidence that the geometry of and chemical effects from the confinement walls do influence the water structure and dynamics, the findings up to date are not building yet to a systematical picture. A representative example is the viscosity of water confined between two hydrophilic surfaces. Major et al.[8] measured a viscosity that is 7 orders of magnitude greater for water under confinement than bulk water. The confinement involved an interfacial separation less than 1 nm between two gold surfaces that were made hydrophilic by the chemisorption of COOH terminated alkanethiol self-assembled monolayer. On the other

hand, Raviv et al. [9] observed a viscosity that is within only a factor of three of its bulk value, when water was under confinement between mica surfaces with an interfacial separation that ranges from 3.5 ± 1 to 0.4 nm or less. The dramatic increase in viscosity in the former was attributed to the hydrogen bonding of water molecules simultaneously to both hydrophilic surfaces, and the persistent fluidity in the latter was interpreted in terms of suppression of the formation of a highly directional hydrogen-bonded networks. Both the observation and the interpretation of the water viscosity in these two hydrophilic interfacial confinement systems exemplify that, while the walls can prominently interfere with the hydrogen bond network in the water, there are important open questions on the aspects of confinement geometry and chemical nature in explaining the confined water properties.

In contrast to this, there are also certain phenomena associated with water confined between hydrophilic walls that are well-established in the literature. A representative example of this category of phenomena is that the water mono-layer in direct contact with the hydrophilic walls are in a glassy state. Inelastic neutron scattering experiments showed that the structure of water in contact with the hydrophilic surfaces of Vycor glass nano-pores at room temperature (298K) is similar to that of bulk supercooled water at 273K.[86] Later on Gallo[2885] et al. showed by molecular dynamics simulation that water molecules residing close to the hydrophilic surface of Vycor glass behaved dynamically as if they were already below the mode coupling crossover temperature although the simulation was performed at room temperature. Another important character for the interfacial water at a hydrophilic surface that is well-known is the increase of long range spatial correlations compared to the bulk liquid water.[86,87]

In this thesis, we pay our attention to a confined water system of both technological and scientific significance. That is the water confined in the interlayer space of a layered hydrated oxide called calcium-silicate-hydrate (C-S-H). This phase precipitates as clusters of nano-scale particles with an associated pore system [8,2,3] as a result of mixing water and cement powder. The pore system evolves during cement setting process from a percolated macro-porous to a micro- and nano-porous structure,[13] in which the smallest pores pose an ultra-confining environment for water between the layers of C-S-H. Cement cohesion,[14] transport of aggressive ions in cement paste[5], concrete creep and shrinkage mechanisms[15,6] are attributed to the chemistry of C-S-H particles and the water between and inside them.

From the scientific perspective, C-S-H offers an interesting ultra-confinement system where both the geometric and the chemical effects of the confinement on water can be probed. In this single-particle C-S-H system, water molecules are trapped mainly in the interlayer space between the highly disordered calcium-silicate layers, forming the so-called interlayer water. A smaller amount of them constituting about 15% of the total water molecules are also trapped in small cavities within the layers, forming the intra-layer water. Besides water, the interlayer space contains calcium ions that neutralize the negative charge of the calcium-silicate layers with a concentration of about three water molecules per calcium ion. This interlayer space has a thickness less than 1 nm and can be pictured as a highly concentrated ionic solution. The ionic solution picture of the interlayer region has been suggested previously for smectites,[18] which are well-crystallized alumino-silicates. The calcium silicate layers in C-S-H have silicate chains that are defective compared to the uniform ones in the calcium-silicate layers of the

crystalline analogue tobermorite. These defects are essentially missing bridging silica tetrahedra. The existence of these defects opens the space in the interlayer region which in turn enhances the connectivity of the pore and increases the possibility for water diffusion[57] as opposed to the situation in the interlayer space in tobermorite. Furthermore, the small distortions in the silicate chains in layered materials can have a greater impact on the dynamics of the nano-confined water than the actual pore size of the confinement as shown by Ockwig [78] et al. using inelastic neutron scattering and molecular simulations. We will discuss the role of the defective silicate chains in our C-S-H system in the results section For illustration purposes, Figure 2.1 depicts a recently reported molecular model of C-S-H[3] that was used in this thesis. Further description of this C-S-H model is given in the Computational Approach section.

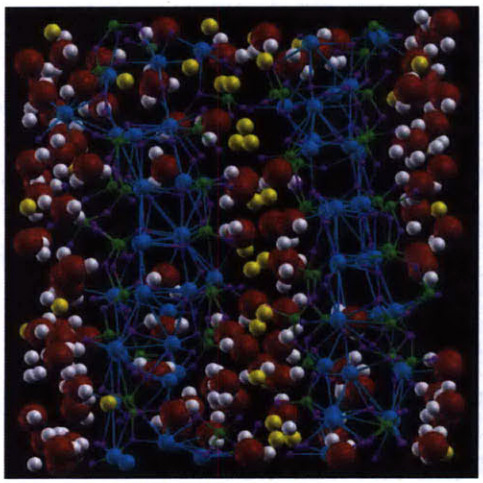

Figure 2.1 A molecular model of C-S-H that encompasses two highly disordered layers of calcium-silicate and water molecules trapped in the interlayer space together with interlayer calcium ions. Few water molecules are trapped in small cavities in the calcium-silicate layers. White spheres are hydrogen atoms, red are oxygen, purple are layer oxygen, green are silicon, light blue are layer calcium and yellow are interlayer calcium. Water molecules are highlighted with a larger size compared to the other elements in the model.

Our objective is to provide a molecular level description of the effect of the disordered and hydrophilic nature of the C-S-H substrate on the properties of water that is quasi two-dimensionally confined between the layers of this substrate. This is important not only for deciphering the nature of water in a realistic confined system, but even more notably for informing the dependencies of the cement paste cohesion and mechanics on the interfacial water structure and dynamics. This in turn, provides directions for science-informed engineering of cementitious materials. In this study we considered the water confined in C-S-H particles rather than water in the large pores capillary that fills the space between the C-S-H particles. The reason for this preference is two-fold: 1) interfacial phenomena has the greatest effect on the structure and dynamics of the molecules that are directly associated with the interface,[21,60,68,81] and 2) starting from the very interfacially confined water and then scaling up to the inclusion of capillary pores would enable to identify the role of water at each scale in the cement cohesion and mechanics.

The focus in this thesis is on the static and dynamic description of confined water. The results are explained in terms of structure, polarization and mobility of water molecules, tying them to a multi-range structure and glassy dynamics that arise in this system. The fact that our model explicitly and realistically [3] accounts for structural disorder in C-S-H means that many of our results can be directly compared to experiments when they become available in the future. The organization of the rest of this chapter is as follows. In section 2.2, the model, force fields and simulation details are described. In section 2.3, numerical results are presented accompanied with discussion

about their indications and significance. Finally in section 2.4, we summarize the major observations and conclusions.

2.2. Computational Approach

2.2.1 Molecular Model

Modeling a material composed of particles with structural disorder in each particle is without a doubt a challenging problem. Recently,[3] a model that takes into account structural disorder for two calcium-silicate layers with the associated interlayer space was developed. As shown in Figure 2.1, the model consists of two sheets of calcium-silicates that entrap water molecules and interlayer calcium cations. The stoichiometric composition of the model is $(CaO)_{1.65}$-(SiO_2)-$(H_2O)_{1.73}$. The cartesian coordinates of the atoms were provided in Reference 12. With periodic boundary conditions in three dimensions, we approximate the C-S-H by infinite layers of disordered calcium-silicates that confine quasi two-dimensional sheets of the water/interlayer calcium solution. This picture is relevant to understand the building block of the cement paste.

2.2.2 Force Fields

We performed the molecular simulation using two different force fields to ensure that the obtained results are most likely realistic and not artifacts due to the method of parameterization. We will refer to the first force field by "core-shell" since it is based on modeling anions polarization by the shell model of Dick and Overhauser.[19] The second force field is the recently developed CSHFF.[20] It is important to note here that many studies[21,22,23] emphasized the importance of including the flexibility and if possible also

the polarizability in modeling water to describe the reactions at an interface or in ionic solution. Famous water rigid models such as the extended simple point charge SPC/E[24] while excellently describe bulk water, they were not able to represent solvation effects of dissolved ions and interfacial phenomena. For example it was shown that the built-in polarization correction of SPC/E makes it too hydrophilic in an interface simulation.[25] In our study, the core-shell force-field incorporates a flexible and polarizable potential for water, while the CSHFF includes a non-polarizable but flexible version of SPC.[26] This means that our results can be regarded also as a tool to evaluate the importance of including flexibility versus polarizability in describing confinement and solvation effects on water in. In fact this was the second purpose of performing our study using two force fields. It will be evident in the results section that the flexibility is sufficient to qualitatively account for these effects with a considerably lower computational cost.

The core-shell force field uses the formal charges for all ions (except water oxygen and hydrogen) and this guarantees charge neutrality of any system under consideration. The parameters of this transferable force field have been optimized by many researchers to study bulk oxides,[29] minerals surfaces[30] and minerals/aqueous solutions interface.[31,32,33] The water component of this force field was originally introduced by de Leeuw and Parker[34] and a major revision for the hydrogen bond representation has been introduced by Kerisit and Parker.[35] On the other hand CSHFF has been developed recently for the family of calcium-silicate-hydrates. It uses optimized partial charges for the ions. It distinguishes between the "layer" calcium and "interlayer" calcium. It also treats the oxygen atoms that bridge two silica tetrahedra differently than the other layer oxygen atoms which do not serve a bridging role. The good agreement

between the CSHFF results and Density Functional Theory predictions was shown for many structural and elastic properties of the minerals 11Å-Tobermorite and 14 Å-Tobermorite.[20]Furthermore, CSHFF was tested against core-shell in predicting structural and elastic properties of the disordered C-S-H phase and the agreement between the two force fields was good.[20]

The advantages and the issues of the two force fields are as follows. Core-shell is proven to be transferable and achieves charge neutrality for any system. However, it is expensive computationally because of the shell representation. It wrongly predicts a density of ~1.3 g/cm^3 for water at ambient conditions. CSHFF is fast computationally, very compatible with the C-S-H family, and has an excellent water potential that predicts a density of ~ 1 g/cm^3 for bulk water at ambient conditions. The credentials of the water component of CSHFF are demonstrated in the results section. However, it does not achieve charge neutrality unless the partial charge of the non-bridging oxygen atoms is slightly modified. The charge modification is always less than 3% for all possible calcium-silicate-hydrate phases. The parameters of both force fields with the real space cutoffs are given in appendix A. Columbic interactions were computed using the Ewald summation method[36] with a precision of 1.0×10^{-8}.

2.2.3 Structure Optimization

The purpose of structure optimization is achieving a reasonable structure that is consequently used in the finite temperature molecular dynamics simulations. In other words, we search for the configuration of the local minimum on the global potential energy surface that the starting coordinates lie closest to. We used the code General

Utility Lattice Parogram (GULP)[37,38,39] to perform the optimization at zero pressure. Second-order Newton-Raphson method as implemented in GULP was used as the energy minimizer. Hessian was updated every step by the scheme of Broyden-Fletcher-Goldfarb-Shanno.[40] When the gradient norm falls below a prescribed value of 0.002, the minimizer was switched to Rational Function Optimization[41] to accelerate the convergence and to generate a stable solution with positive eigenvalues of the Hessian matrix.

2.2.4 Molecular Dynamics

Finite temperature molecular dynamics (MD) was used to study the equilibrium structure, polarization, and dynamical properties for both bulk and confined water. The code DL_POLY_2[42,43] was used to perform the simulation. For core-shell simulations, we treated the shells using the adiabatic approach described by Mitchell and Fincham,[44] whereby the shells were assigned a small mass of 0.2 atomic mass unit. Based on this mass and the core-shell spring constants given in appendix A, the vibrational frequency of the core-shell unit in the layer oxygen and water oxygen were found to be around 10000 cm^{-1} and 17000 cm^{-1} respectively. This means that they are well above the highest vibrational frequency in the system which is the O-H bond stretching that is around 3300 cm^{-1}. This is sufficient to prevent effective kinetic energy exchange between the core-shell unit and the remaining system.

Bulk water was represented by 537 molecules in a cubic cell. C-S-H initial configuration was taken from Reference 12 and has been doubled in the direction of the shortest cell vector to allow better sampling statistics for the equilibrium properties for confined water which is represented by 208 molecules. After energy minimization,

isobaric-isothermal (NPT) simulations were performed for 1 ns with a target pressure and temperature of zero atmosphere and 300 K, respectively. During these simulations, configurations with cell vectors close to the average equilibrium values were taken and used to start canonical ensemble (NVT) simulations. All systems were equilibrated in the NVT ensemble for 250 ps, followed by 1 ns of production. A time step of 0.1 fs was used (unless otherwise stated). Thus, each production run corresponds to $1x10^7$ time steps. Berendsen method was used to control both the pressure and temperature with a relaxation time of 0.5 ps for both the barostat and the thermostat. In all simulations, equations of motion were integrated using Verlet-Leapfrog algorithm. Trajectories were recorded every 10 fs.

2.3 Results and Discussion

This section is presented in three subsections. First, we examine the nature of the interaction between the confined water and C-S-H in terms of hydrophilcity and hydrophobicity. Second, we elaborate on the structure of the confined water in C-S-H and compare it to bulk water. Our comparison criteria are the doublet and triplet correlations. The Triplet correlations show similarity between the confined water structure and the structure of dense fluids and supercooled phases. This provided us with the evidence that the confined water can behave dynamically as a glassy material. In the third part we examine, and eventually demonstrate, the glassy nature of the confined water in this quasi two-dimensional hydrophilic system.

.2.3.1 Hydrophilicity of C-S-H substrate

Characterizing the C-S-H substrate in terms of hydrophilicity and hydrophibicity provides the first step in understanding the nature of the interaction between the confined water and the calcium-silicate layers in the presence of interlayer calcium cations. To reveal this attribute, we examined the atomic density profile of oxygen (Ow) and hydrogen (Hw) of water in the direction normal to the plane of the calcium-silicate layers denoted as C-S. The profiles are shown in Figure 2.2.

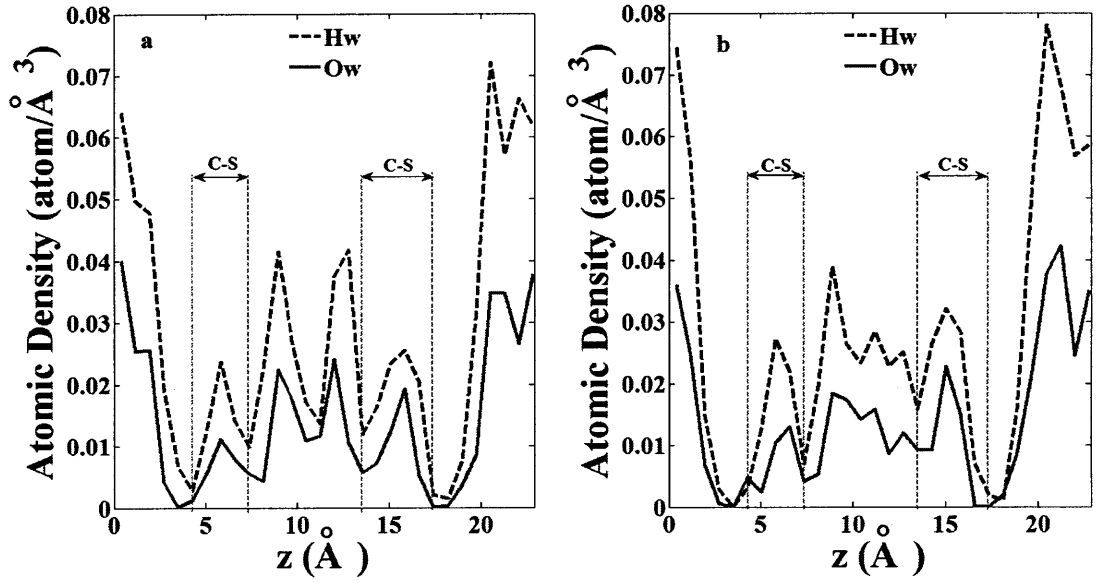

Figure 2.2 Atomic density profile of water hydrogen (Hw) and water oxygen (Ow) in the direction normal to calcium-silicate layers. (a) Using the CSHFF force field. (b) Using the core-shell force field. C-S denotes the position of the calcium-silicate sheets.

From the profiles in Figure 2.2, two pores of thicknesses that range from ~6 to ~9.5 Å are evident. The first pore extends from $z \approx 7.5$ Å to $z \approx 13.5$ Å while the second extends from $z \approx 17.5$ Å to $z \approx 23$ Å and continues under periodic boundary conditions from $z \approx 0$ Å to $z \approx 4$ Å. The peaks that appear around $z \approx 5.5$ Å and $z \approx 15$ Å are due to

water molecules trapped in small cavities in the calcium-silicate (C-S) layers. The hydrogen density profiles show that water molecules prefer pointing their hydrogen towards the calcium-silicate layers to form hydrogen bonds with the layer oxygen. This is the first signature of the hydrophilicity of the C-S-H layers.

In cationic clays which are crystalline layered materials that have silicate chains grafted on the layers and cationic solution in the interlayer space similar to the situation in C-S-H, it is known that the grafted well-crystallized silicate chains are slightly hydrophobic.[59] The main reason for this is that most of the oxygen atoms in the silicate chains in a crystalline material occupies bridging sites and are not available to form hydrogen bonds with the interlayer water. On the other hand in C-S-H, the disorder has a significant impact on its hydrophilicity. The finite length silicate chains which are mainly dimers allow substantial amount of non-bridging oxygen atoms that provide acceptor sites for hydrogen bonds to the interlayer water, rendering this interface a hydrophilic one.

Another metric we used to characterize the nature of the interaction between water and C-S-H is the distribution of the single water molecule dipole moment magnitude. This exploits the fact that water molecules have a permanent electric dipole moment. The dipole magnitude distribution is sensitive to the environment in which water molecules exist, and an up-shift of the dipole distribution would correspond to the hydrophilicicty of the C-S-H confinement interface. We considered this distribution for the bulk and confined water and the results are shown in Figure 2.3. Before discussing the effect of confinement by C-S-H on the water dipole distribution, we examine the bulk

liquid average dipole magnitude for both force fields. The flexible SPC and core-shell predict an average value of 2.44 D and 1.90 D, respectively.

The value of water dipole in the liquid state has been rarely reported experimentally. Badyal et al.[61] employed x-ray diffraction and deduced indirectly that the dipole moment of a liquid state water molecule is 2.9 ±0.6 D. On the other hand Puibasset and Pellenq[4] showed from Hartree-Fock calculations that the value of a single water molecule dipole is very sensitive to the simulation details. For an HOH angle of 109.45^0 and OH bond length of 1 Å represented by the rigid SPC geometry, they found a water dipole of 1.67 D using the 6-31G* basis set, and 0.7 D using the STO3G basis set. On the other hand, this geometry is supposed to correspond to a dipole of 2.245 D in classical molecular dynamics. A similar conclusion was arrived to by Dyer and Cummings[70] for the single water dipole in the liquid state using Car-Parrinello *ab initio* molecular dynamics at 300 K. Using two different techniques to analyze the simulation results; they obtained two values, 2.5 D and 3.1 D.

Given these uncertainties, we think that the predicted values from our classical force fields in our results, particularly those from the flexible SPC fall in a reasonably consistent range in comparison with prior reports. For confined water in C-S-H, both force fields predict a positive shift to larger values of the dipole moment compared to that of bulk water. For CSHFF the shift is about 0.07 D (~2.9 % of bulk value), while for core-shell it is about 0.09 D (~4.7 % of bulk value).

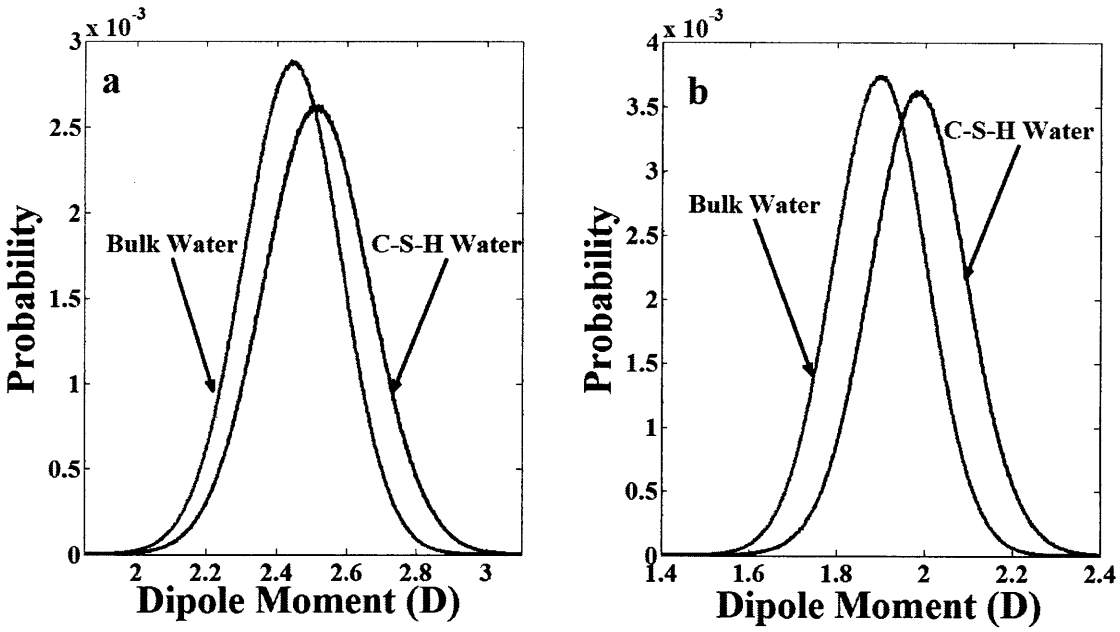

Figure 2.3 Distribution of the dipole moment of the single water molecule, using (a) CSHFF, (b) core-shell.

This upshift of the dipole magnitude distribution is another signature of the hydrophilicity of the C-S-H layer surface. For confined water in a hydrophilic framework, this upshift is due to the large electric field induced by the framework that polarizes the water molecule to an extent larger than the self-polarization in the normal liquid water.[69] For example, a similar upshift in the dipole distribution was observed in a molecular dynamics simulation for water confined in a hydrophilic zeolite, using a fluctuating charge SPC water model.[52] On contrary, water confinement in a hydrophobic framework lowers the water dipole moment distribution compared to bulk.[4,69]

For layered materials with ionic solution in the interlayer space, there is a delicate balance between the nature of the layers and the identity of the ion in the interlayer space. This balance determines the domain in which these materials belong to, hydrophilic versus hydrophobic.[59] For the C-S-H/water system we showed that the interaction is hydrophilic and pointed out that the disordered silicate chains plays a role in biasing the system towards hydrophilicity. Added to this, the interlayer cation in C-S-H system, Ca^{2+}, works in the same direction. In other words, both the layers and the interlayer calcium enhance the hydrophilic nature of the interaction in C-S-H/water system.

The hydration shell structure around the interlayer calcium provides a driving force for the sorption of water into the interlayer space. Not only the interlayer calcium facilitates the sorption of water molecules in the interlayer space, but it contributes to the strong electric field that polarizes the water molecules as well. To provide a quantitative basis for our description of the role of the interlayer calcium, we calculated the mean dipole moment of the water molecule as a function of the distance between interlayer calcium (Cw) and water oxygen (Ow). This is shown in Figure 2.4, accompanied by the radial distribution function $g_{CwOw}(r)$ in the insets.

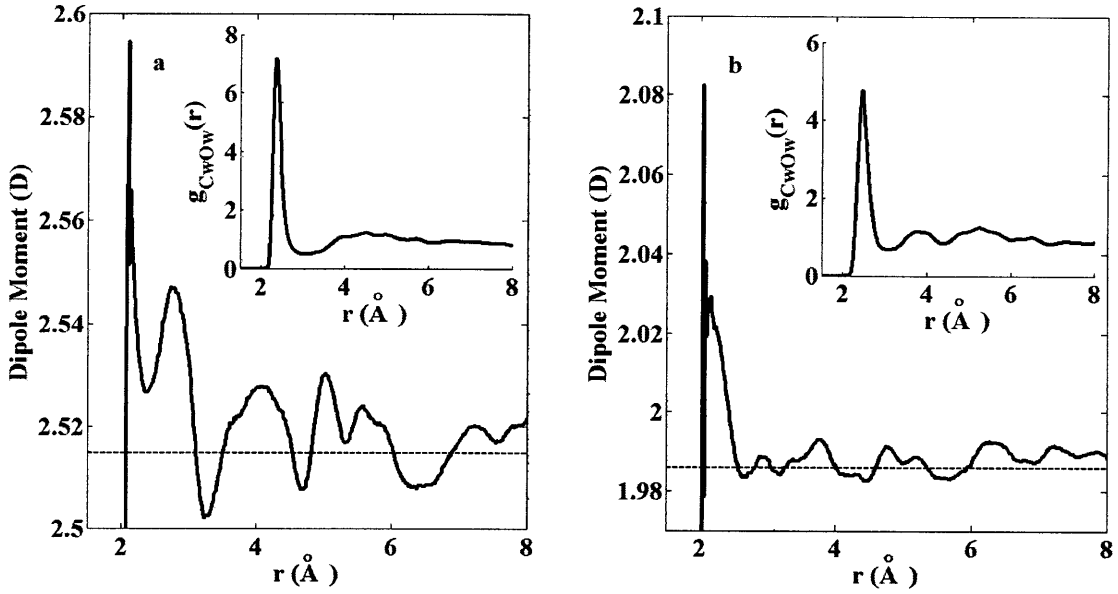

Figure 2.4 Mean water molecule dipole moment as a function of the distance between the interlayer calcium (Cw) and water oxygen (Ow), using (a) CSHFF, (b) core-shell. The radial distribution function $g_{Cw\text{-}Ow}(r)$ is shown in the insets. Dashed lines correspond to the mean dipole of the water molecule confined in C-S-H.

According to the resulting distribution using CSHFF, there is a well defined first hydration shell for water molecules around the interlayer calcium but the second shell is not clear. Core-shell, however, shows two distinguished hydration shells. Both force fields predict an increase (by 0.06 D for CSHFF and 0.1 for Dcore-shell) in the average molecular dipole at very close separation between the water molecule and the Ca^{+2} cation. By the end of the first hydration shell in the radial distribution function, the molecular dipole reaches the mean value for the confined water and oscillates around it. Since the concentration of the interlayer calcium in the confined water is very high, one Ca^{+2} cation per three water molecules, we believe that the overall distribution of the water dipole (Figure 2.3) is significantly influenced by this. The increase of water dipole near a cation in general, and Ca^{2+} in particular, was observed by classical and first

principles simulations,[53,54,55,56] supporting our results. For example, Lightstone et al.[55] reported using Car-Parrinello molecular dynamics an increase in the first hydration shell of Ca^{2+} by 0.2 D.

At this point, we also infer about the nature of the two force fields under consideration. While a flexible and polarizable model such as the core-shell could be expected to be more sensitive for replicating the effects of confinement and ion solvation on the water molecule dipole, our simulation results showed that a flexible and non-polarizable model as this version of SPC was sufficient to capture the same effects qualitatively with much lower computational cost. Our results clearly support the sufficiency of flexibility in the water model to account for the confinement and solvation effects on water molecules in the C-S-H model.

2.3.2 Multi-Range Structure of Confined Water

Elucidating the structure of a confined fluid requires careful examination of the spatial correlations between the molecules. For a polar molecule as water, considering both the site-site and dipole-dipole correlations is an asset. Typically the two-body site-site correlations as epitomized in the partial radial distribution functions are the most studied ones for liquids because of the possibility of direct comparison with neutron and x-ray scattering experiments. However, limiting the analysis to two-body correlations leaves considerable uncertainty in determining the geometrical structure. Extending the analysis to three-body correlations and even higher orders is tractable theoretically but the lack of direct comparison with experiments limited such extension in literature. We report here the two- and three-body correlations for confined water in C-S-H. Recent

advances in x-ray absorption experiments[51] and inelastic neutron scattering experiments[49] allowed direct information on triplet correlations. This means that it is possible now to draw comparison between theory and experiments in terms of triplet correlations, and the triplet correlations that we predict and present here can motivate experimental investigation of the same correlations in water confined in C-S-H.

We begin our analysis for the confined water structure by calculating the partial radial distribution functions, shown in Figure 2.5 for the oxygen-oxygen (OwOw), oxygen-hydrogen (OwHw) and hydrogen-hydrogen (HwHw) correlations. The peaks due to the intramolecular interactions have been omitted. In this figure, we compare the results obtained by the simulations for both bulk and confined water with the experimentally determined data of these functions for bulk water taken from reference 46 by Soper and Philibs. The differences in peak heights and minima depths between the bulk and confined water radial distribution functions determined by simulations are mainly due to the inaccuracy of the volume used in the normalization for the confined water. The bulk water completely fills the simulation cell volume while the confined water occupies a fraction of the simulation cell and it is difficult to quantify this fraction.[45] However, the differences in the peaks and minima positions and widths between the bulk and confined water are real and due to the chemistry and geometry of the confining environment, and thus, are important to notice. Table 1 shows these values and allows for a direct comparison. The coordination numbers were calculated using the definition: [45]

$$N = 4\pi \frac{N_\beta}{V} \int_0^{1^{st}\,\mathrm{min.}} g_{\alpha\beta}(r) r^2 dr, \tag{2.1}$$

where N_β is the total number of β atoms in the system and V is the volume of the simulation cell. The integration is carried up to the first minimum, denoted as '1^{st} min.'.

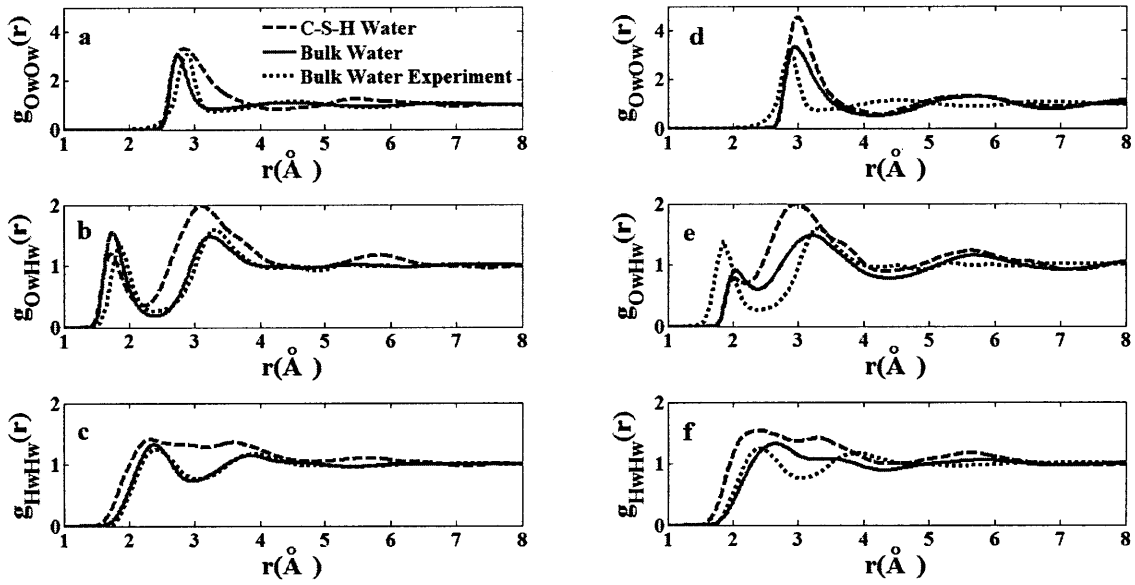

Figure 2.5 Radial distribution functions for the bulk and confined water. CSHFF results are in a, b, and c. Core-shell results are in d, e, and f. Experimental results for bulk water were taken from reference 46. The legend applies to both force fields and to all radial distribution functions.

Table 2.1 The first peak position, the first minimum position, and the intermolecular coordination number in the first shell denoted by N.

	First Peak (Å)	First minimum(Å)	N
	Ow-Ow		
Bulk Water (CSHFF)	2.75	3.33	4.50
Confined Water (CSHFF)	2.85	4.23	5.69
Bulk Water (Core-Shell)	2.96	4.17	12.88[a]
Confined Water (Core-Shell)	3.00	4.26	5.58
Bulk Water (Experimental)[46]	2.88	3.33	4.63[b]
	Ow-Hw		
Bulk Water (CSHFF)	1.73	2.41	1.89
Confined Water (CSHFF)	1.72	2.21	0.62
Bulk Water (Core-Shell)	2.04	2.39	1.98
Confined Water (Core-Shell)	2.02	2.21	0.39
Bulk Water (Experimental)[46]	1.85	2.35	1.76[b]
	Hw-Hw		
Bulk Water (CSHFF)	2.39	2.96	5.44
Confined Water (CSHFF)	2.35	2.69[c]	2.09

Bulk Water (Core-Shell)	2.64	3.29	11.42[a]
Confined Water (Core-Shell)	2.42	2.98	3.46
Bulk Water (Experimental)[46]	2.45	3.05	6.04[b]

a These over-estimated coordination numbers are due to the large broadening of the first peak and the high density inaccurately predicted for the bulk water by the core-shell force field.

b We have calculated these numbers from the radial distribution functions reported in reference 46.

c There is no clear first minimum in Figure 2.5-c, however, at $r = 2.69\,Å$ there is some distinction between the first peak and a neighboring shoulder that we noted here.

It is evident that the water potential in CSHFF is superior in predicting the structure of bulk water as it agrees reasonably well with the experiment. The core-shell significantly broadens the first peak in the oxygen-oxygen and hydrogen-hydrogen correlation functions which, together with the fact that it predicts higher bulk water density, leads to an overestimation of the corresponding coordination numbers.

For confined water, CSHFF predicts that the oxygen-oxygen spatial correlations are extended to a larger distance as indicated by ~0.9Å shift of the first minimum and a shift in the second peak of ~1Å in $g_{O_wO_w}(r)$. This is accompanied by a larger coordination number in the first shell. An explanation for this larger coordination will be given later after examining the triplet correlations. On the other hand, the core-shell predicts a much smaller shift to a larger distance of the first minimum of about ~0.1Å. On contrary to CSHFF, it predicts a shift to a shorter distance of the second peak of about ~0.2Å and predicts a reduction in the coordination number. The reason behind this discrepancy is that the second peak predicted by the core-shell potential is already shifted to a larger

distance in bulk water compared to the experiment and it also exaggerates the coordination number in bulk.

Both force fields predict the same behavior of the oxygen-hydrogen correlations for confined water in C-S-H. The major feature is the reduction in the coordination number which can be translated as a reduction in the number of hydrogen bonds among water molecules. This is the consequence of the available donor bonds of water molecules that are donated especially to the non-bridging oxygen atoms on the calcium-silicate layers. . In addition to this, the second peak in $g_{OwHw}(r)$ that corresponds to the farther hydrogen atom in a neighboring water molecule is broadened towards shorter distances. It is interesting also to note that the third peak, especially by CSHFF results, is more pronounced than the third peak in bulk water This shows that the site-site spatial correlations persist up to long distances for confined water.

The hydrogen-hydrogen radial distribution function for the confined water is very different than bulk. Both potentials show that the first peak is broadened towards shorter distances. They also predict that the first and second peak merge together. Moreover the third peak becomes more pronounced compared to bulk. These deviations in the three correlation functions for the confined water compared to bulk show signs of the distortion of the tetrahedral netwrork of water when confined between the C-S-H layers and are attributed to : 1) the effect of the disordered hydrophilic calcium-silicate sheets that offers significant number of acceptor sites for hydrogen bonds to the confined water, 2) The strong interlayer calcium slovation effects (see Figure 2.4), and 3) The quasi-two-dimensional confining geometry imposed by the substrate.

As we mentioned earlier, the permanent polarity of water molecules allows the dipole-dipole spatial correlations to be a useful tool to probe the local structure, especially the orientational correlations. In order to exploit this tool to provide more details about the structure of confined water in C-S-H, we computed the dipole-dipole correlation function for the bulk and confined water. This function is defined as:[62]

$$h_{OwOw}(r) = 3g_{OwOw}(r) < \cos \vartheta >, \qquad (2.2)$$

where θ is the angle between the dipole vectors of two water molecules at an oxygen-oxygen distance, r. The calculated functions are shown in Figure 2.6 accompanied with $g_{OwOw}(r)$ for comparison.

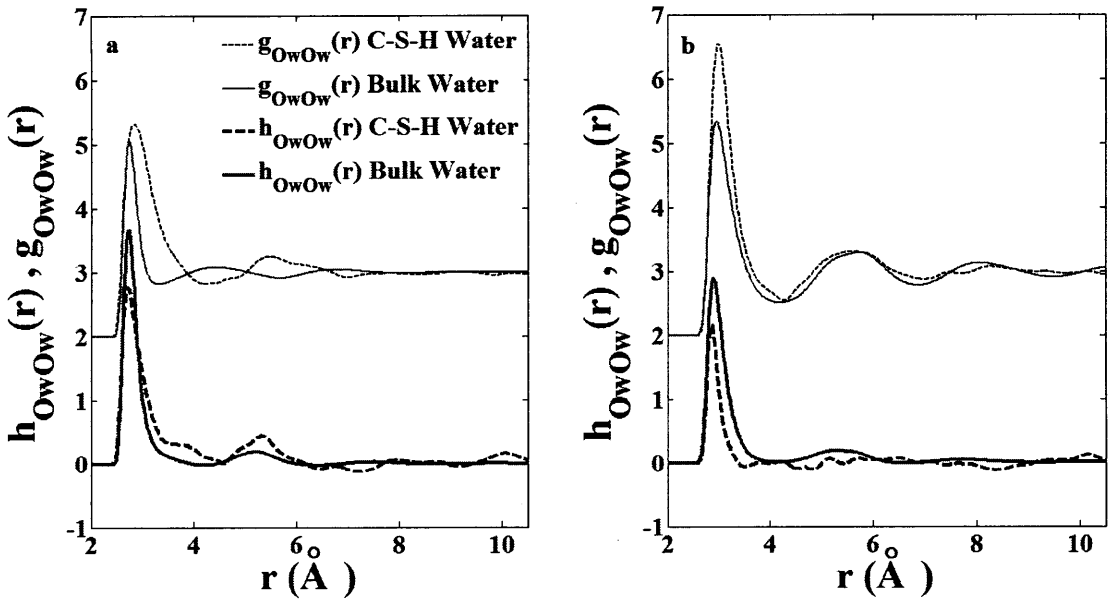

Figure 2.6 The oxygen-oxygen radial distribution function, $g_{OwOw}(r)$ (top thin lines) and the dipole-dipole correlation function, $h_{OwOw}(r)$ (bottom thick lines) as a function of oxygen-oxygen distance, r, using (a) CSHFF and (b) core-shell. The legend in (a) applies to results from both force fields. The positive values of $h_{OwOw}(r)$ correspond to correlated dipole moment vectors, while negative values correspond to anti-correlated ones.

Comparing $h_{OwOw}(r)$ and $g_{OwOw}(r)$ for bulk water shows that both functions continues to exhibit correlations up to 7-8 Å. The confinement extends the correlations in $h_{OwOw}(r)$ of water in C-S-H up to 10 Å. It is also interesting to note the negative value minimum at 7.5 Å (CSHFF) and at 8 Å (core-shell) in the plot of $h_{OwOw}(r)$ for confined water. Such a negative value minimum corresponds to anti-correlated dipole moment vectors. Cross-talk of water molecules from the separated pores of C-S-H does not interfere with these $h_{OwOw}(r)$ results, because similarly extended correlational behavior is evident when the same calculations are performed by constraining the search only to a two-dimensional single pore of water in the model. Overall, these long range dipole-dipole correlations demonstrate that the orientational correlations in the confined water in C-S-H persist considerably at longer distances than in bulk water.

We attribute the origin of these long-distance correlations to two possible mechanisms. First is the directional hydrogen bonding formed between the confined water molecules and the defective silicate chains that provides substantial amount of acceptor sites through the non-bridging oxygen atoms. The role of the directional hydrogen bonding in enhancing orientational correlations was similarly shown[79] for the hydroxyl groups of sugar alcohols. Second, is the increase of the number of correlated molecules and spatial correlations as the temperature of a supercooled liquid decreases approachig the glass transitions, recently demonstrated by Crauste-Thibierge[80] We will show later in this chapter that this confined water behaves in a glassy fashion similar to that of supercooled liquids as if it has an effective temperature lower than the actual temperature, enabling the persistence of long range correlations. In fact there might be synergistic interference between these two mechanisms that we propose here, since the

observation made by Crauste-Thibierge[80] et al. was based on studying supercooled glycerol whose molecules are also hydrogen bonded directionally by hydroxyl groups.

By combining the observations above from the two-body correlations together, and prior to considering the three-body correlations, we deduce that the local tetrahedral structure of water is distorted when confined in a disordered hydrophilic layered material such as the C-S-H. However, some correlations are enhanced and extend to longer distances for the confined water compared to bulk.

Having examined the two-body correlations thoroughly, we turn our attention to the triplet correlations in order to depict more precisely the local structure of confined water. The oxygen-oxygen-oxygen (OwOwOw) angular distribution for the neighboring oxygen atoms in water is what we report for this purpose. To calculate this distribution, we define two oxygen atoms to be neighbors if they are separated by a distance less than a certain cutoff distance. This cutoff distance, r_{cut}, is usually taken as the position of the first minimum, r_{min}, in $g_{OwOw}(r)$ (see Figure 2.5). Instead of calculating the (OwOwOw) angular distribution only at r_{min}, we varied this cutoff between r_{min} and fractions of it, as $r_{cut}=f.r_{min}$, $0<f<1$. This serves to search for the oxygen-oxygen separation less than which the bulk tetrahedral structure signatures remain in the confined water. Based on this search we determined a critical cutoff distance for each force field and for both bulk and confined water that represents the range over which the tetrahedral coordination extends.

In Figure 2.7 we demonstrate the search process by varying the cutoff for the case of bulk water using CSHFF where we plot the (OwOwOw) angular distribution as a function of the cutoff distance (r_{cut}) and the angle between the three oxygen atoms (OwOwOw Angle). In Figure 2.8 we show the same distribution for both force fields, for

bulk and confined water, and by a cutoff at the first minimum, r_{min}, in $g_{OwOw}(r)$ and the critical one that we determined by the search process

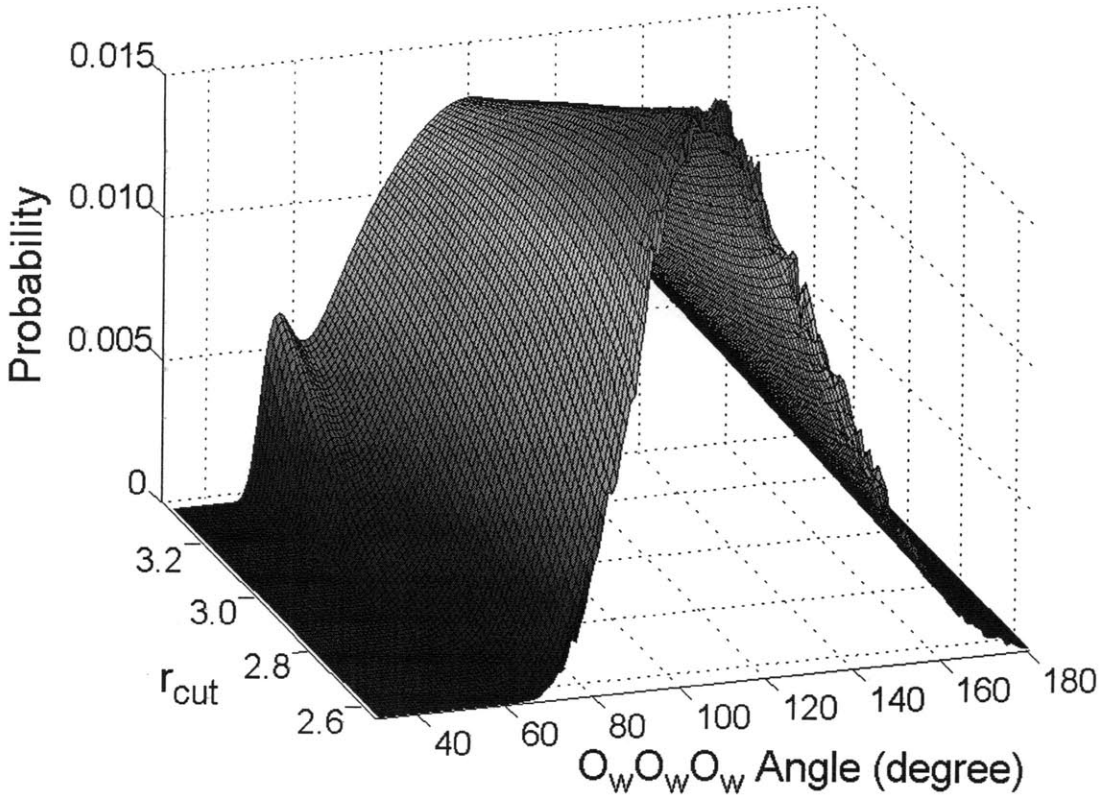

Figure 2.7 The distribution of the oxygen-oxygen-oxygen (OwOwOw) angle between the oxygen atoms in three neighboring water molecules as a function of the angle and the search cutoff distance, r_{cut} . The plot is for bulk water using CSHFF. The figure illustrates how the critical cutoff that corresponds to the range over which the tetrahedral structure is obtained.

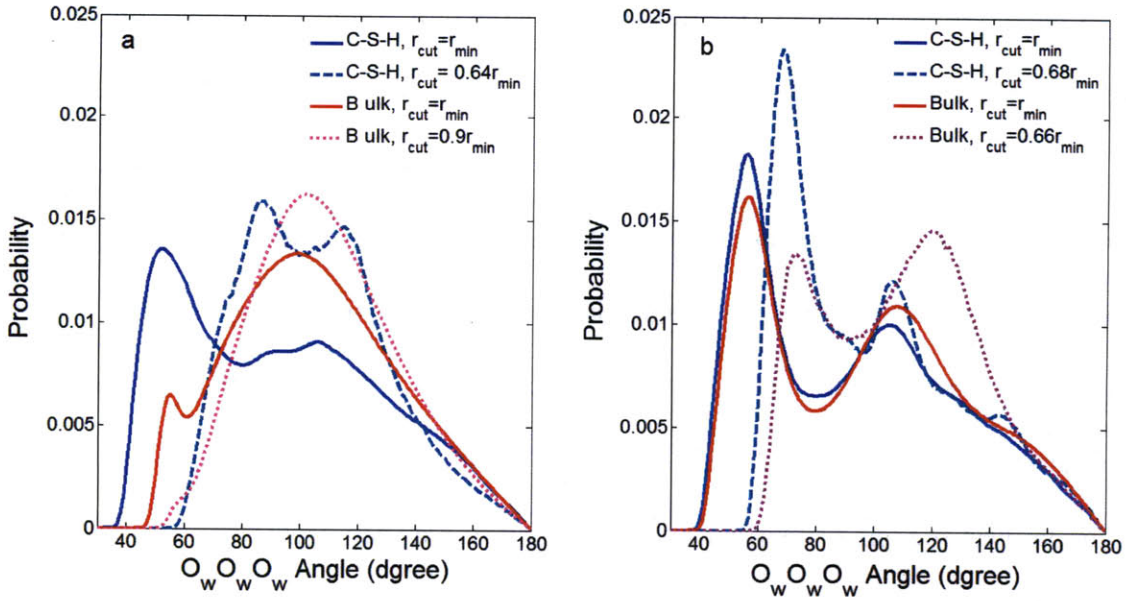

Figure 2.8 The distribution of the oxygen-oxygen-oxygen (OwOwOw) angle between oxygen atoms in three neighboring water molecules, (a) using CSHFF, and (b) using core-shell. $r_{cut}=r_{min}$ corresponds to the usual cutoff which is the first minimum in $g_{OwOw}(r)$. The plots corresponding to $r_{cut}=f.r_{min}$, $0<f<1$, were determined by search for the appropriate fraction, f, that eliminates the interstitial water molecule peak (CSHFF) or at least shifts it to higher values (core-shell).

In bulk water, this distribution is characterized by an intense and broad peak near the tetrahedral angle of 109° and a smaller peak at ~55°.[49] The peak at 55° is due to the angle between an interstitial water molecule in the first shell of a central molecule and a tetrahedral neighbor. By setting the cutoff to r_{min}, we found that the CSHFF was able to reproduce these features accurately for bulk water, while the core-shell overestimated the relative probability of the interstitial peak compared to the peak at the tetrahedral angle. This overestimation by core-shell is the reason for the high density and large coordination numbers predicted by this potential for bulk water at ambient conditions since this interstitial peak manifests itself as dense packing of water molecules. On the other hand both force fields agree in predicting the enhancement of the interstitial molecule peak for

water under confinement in C-S-H relative to that in bulk water. This enhancement is the origin of the observed larger coordination number of water molecules in the first shell of $g_{OwOw}(r)$ predicted by CSHFF (see Table 2.1) for confined water. Moreover the tetrahedral peak is reduced and narrowed. When we change the cutoff to distances to less than r_{min}, we observe several interesting characteristics. For bulk water using CSHFF we determined a critical value of $r_{cut}=0.9r_{min} \approx 3.00\text{Å}$, at which the interstitial water molecule peak disappears (see Figure 2.7 and Figure 2.8). This indicates that the interstitial site is in the farthest regions of the first hydration shell, more specifically between 3.00Å and 3.33Å. On the other hand, for confined water modeled using the CSHFF the interstitial molecule peak keeps approaching the tetrahedral peak until the search cutoff reaches a lower critical value of $r_{cut}=0.64r_{min}\approx 2.72$ Å. At this distance. it joins the tetrahedral peak and the latter gets enhanced (see Figure 2.8). This finding showed us that the tetrahedral order is still prevails up to shorter distances (~2.72Å) in this confined water compared to bulk water (~3.00Å) but it is slightly distorted. Such piece of information was not available from our examination of the two body correlations but became clear by a careful study of the OwOwOw angular distribution.

Core-shell predictions for the radial distribution functions for bulk water were acceptable but not as accurate as that of CSHFF. In the triplet correlations, it was only able to qualitatively capture the trends that CSHFF followed for confinement effects. We determined a cutoff for bulk core-shell water of $\sim 0.66r_{min}\approx 2.75\text{Å}$ at which the interstitial molecule peak shifts significantly to higher angles and gets closer to the tetrahedral angle peak. The latter also gets enhanced and becomes comparable to the interstitial molecule peak. A similar cutoff has been determined for confined water at $\sim 0.68r_{min}\approx 2.90\text{Å}$ at

which the intestinal peak marginally shifts to higher angles and the tetrahedral peak marginally increases indicating that there are still some remnants of the tetrahedral coordination . In addition to this another structural feature appears at angles between 140^0-160^0.

Recently Strassel et. al. [50] showed that bulk water at a temperature of 670 K and a pressure of 6.5 GPa exhibits a similar angular distribution as the one shown here for confined water by setting $r_{cut}=r_{min}$ - similar in the sense that the tetrahedral peak diminishes and the interstitial molecule peak gets enhanced. This distribution was also shown to be obeyed by a simple dense Lennard-Jones liquid[50] and by undercooled and liquid copper.[51]Such similarity in the triplet correlations between these dense phases and the confined water in C-S-H under consideration here gave us a tantalizing evidence that this confined water could behave dynamically in a glassy fashion. In section 2.3.3 we elaborate more on this.

From the results presented in this section, we draw an overall picture of the structure of confined water in C-S-H with three major components at three length scales. First, at short distances the tetrahedral coordination between water molecules is still intact. Second, at intermediate scale (up to the distance of first minimum in $g_{OwOw}(r)$), water molecules adopt a structure similar to that of dense fluids and supercooled phases. Finally, at large distances (up to 10 Å) dipole-dipole correlations remain significant. This, in turn, imposes a highly correlated orientational motion for the molecules.

As far as the structural properties that we considered in this section, we believe that CSHFF with its superior flexible SPC water potential predicts more reliable

confinement effects compared to the core-shell. Our confidence is mainly built on its good performance in reproducing bulk water properties and the fact that the whole force field CSHFF is tailored for the family of calcium-silicate-hydrate compounds.

2.3.3 Glassy Dynamics of Confined Water in C-S-H

As evidenced from the triplet correlations in the previous section, the water confined in C-S-H exhibits structural characteristics similar to those in dense fluids and supercooled phases. It is also known that the glassy behavior of materials manifests itself more pronouncedly in the translational dynamics, and is characterized by three stages initiated by the ballistic motion at short time scales, followed a cage behavior slowing down the motion at intermediate scales, and finally the diffusive motion at long time scales.[64] We investigated the mean square displacement (MSD) of the oxygen atoms in water in order to test our assertion about the glassy behavior of confined water in C-S-H. Due to the quasi-two dimensional geometry of the C-S-H ultrafine confinement, we calculated not only the three dimensional MSD, but also the two dimensional MSD parallel to the calcium silicate sheets and the one dimensional MSD perpendicular to those sheets. Utilizing invariance under time translation, the mean square displacement, MSD, was calculated using:

$$\left\langle \Delta \underline{r}^2(t) \right\rangle = \left\langle \frac{1}{N} \sum_{i=1}^{N} \left| \underline{r}_i(t+\tau) - \underline{r}_i(\tau) \right|^2 \right\rangle, \qquad (2.3)$$

where $\underline{r}_i$ is the coordinate of the i^{th} oxygen atom in water, and the brackets denote averaging over multiple time origins, τ. The results of the calculations are plotted on a log-log scale and shown in Figure 2.9. The MD simulation of the confined water using

CSHFF was also performed for 5 ns using a longer time step of 0.5 fs to reveal all three stages of glassy dynamics. Such a long time step was not affordable by the core-shell force field because of the fast vibrations of the core-shell unit that limit the time step to small values. Nevertheless, all three stages are also evident using the core-shell force field in water confined in C-S-H already up to 1ns simulation time.

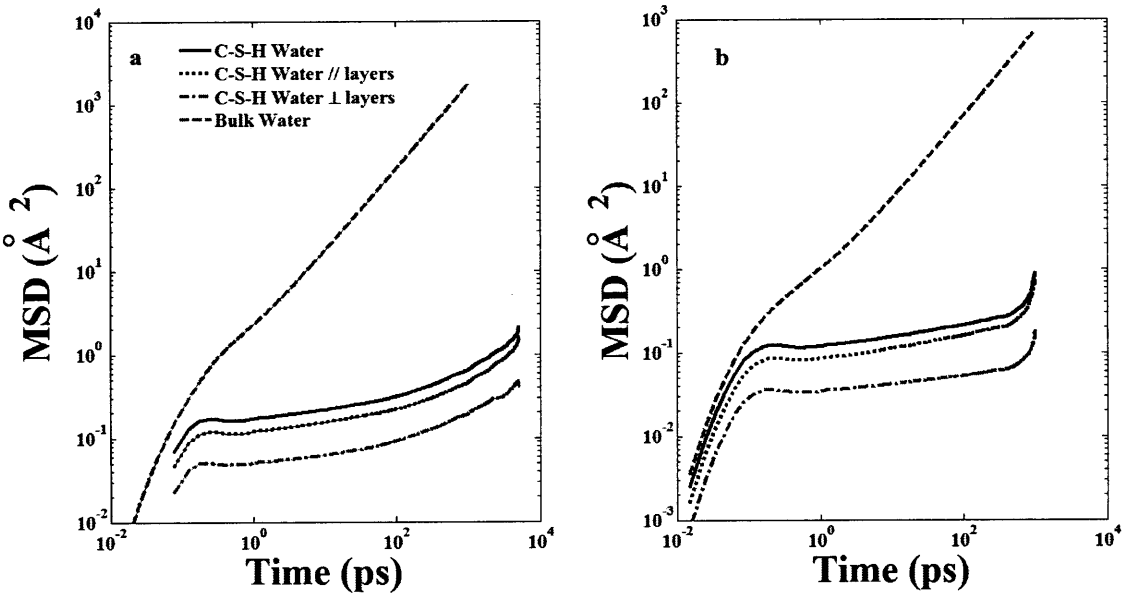

Figure 2.9 The mean square displacement for the oxygen in bulk and confined water, (a) using CSHFF and (b) using core-shell. The legend in (a) applies to both force fields.

For bulk water, using both force fields for t < 0.4 ps, there is an early-stage parabolic jump followed by a linear behavior that is typical for liquids. For confined water in C-S-H, we observe the three stages of glassy dynamics. First, for both potentials and at short times, t < 0.4 ps, a ballistic motion prevails, with MSD proportional to t^2, since the motion of the water molecule is not yet affected by the presence of other molecules or atoms surrounding it. Second, between $t = 0.4$ ps and $t \approx 400$ ps for both

potentials, the water molecule starts to collide with its neighboring molecules and atoms, thus it only rattles in the cage formed by the surrounding molecules. The water molecules participating in forming this cage are themselves in cages surrounding them as well. All motion is slowed down for about three decades in time regime. Then, the molecules succeed in escaping the cage and undergo diffusive motion, with MSD proportional to *t*. Both force fields agree qualitatively on these three stages. However, the onset of diffusive motion is very clear for core-shell, while the transition from the cage region to the diffusive region is gradual for CSHFF and there is no sharp transition point. This is the reason behind performing 5 ns simulation for the confined water using CSHFF. Demonstration of these three stages of glassy dynamics supports our hypothesis that we deduced from the intermediate range structure of confined water in section 2.3.2.

In addition to the glassy dynamics, the MSD shows that at early stages, the molecular displacement for water is almost isotropic in all directions. Later on when the diffusive motion is initiated the value of the MSD parallel to the calcium-silicate layers (black dotted curve) approaches the value of the three dimensional MSD (blue line) in Figure 2.9. This supports the quasi two-dimensional character of the ultra-confinement environment of water between the calcium-silicate sheets. The two-dimensional diffusion is enhanced by the connectivity in the ultra-thin interlayer space allowed by the defective silicate chains. Without this connectivity, the only motion available to water molecules would be the vibrations and restricted rotations as in the case of the crystalline analogues of C-S-H.

There are universal features that govern the slow dynamics of glassy materials.[47] In addition to the MSD, a major feature that directly relates to the translational dynamics

is the non-Gaussian behavior of the self-part of the van Hove function. The origin of this non-Gaussian behavior is usually attributed to dynamical heterogeneity that involves cooperative motion of neighboring particles.[48] This heterogeneous dynamics has been observed in the case of dense two-dimensional glass-forming systems both experimentally[71,72] and by simulation.[73] To further support the glassy dynamics of the water confined in the quasi two-dimensional C-S-H discussed above, we quantified its deviation from the non-Gaussian behavior or in other words its dynamical heterogeneity. This is achieved by calculating a time-dependent non-Gaussian parameter (NGP) of the form: [63,82]

$$\alpha_n(t) = \frac{\left\langle \Delta \underline{r}^{2n}(t) \right\rangle}{C_n \left\langle \Delta \underline{r}^{2}(t) \right\rangle^{n}} - 1, \qquad (2.4)$$

$$C_n = 1 \times 3 \times 5 \times 7 \ldots\ldots (2n+1)/3^n,$$

for n = 2, 3, 4, ... Time average is denoted by $\langle \ldots. \rangle$, $\Delta \underline{r}^2(t)$ is the mean square displacement and $\Delta \underline{r}^{2n}(t)$ is the mean $2n$ displacement. The non-Gaussian behavior is characterized by non-vanishing $\alpha_n(t)$. For the purpose of our study we utilized only $\alpha_2(t)$ as our NGP. The results of the calculated NGP for the oxygen atom of bulk and confined water using both force fields are shown in Figure 2.10. For CSHFF the confined water result is shown for the 5 ns simulation.

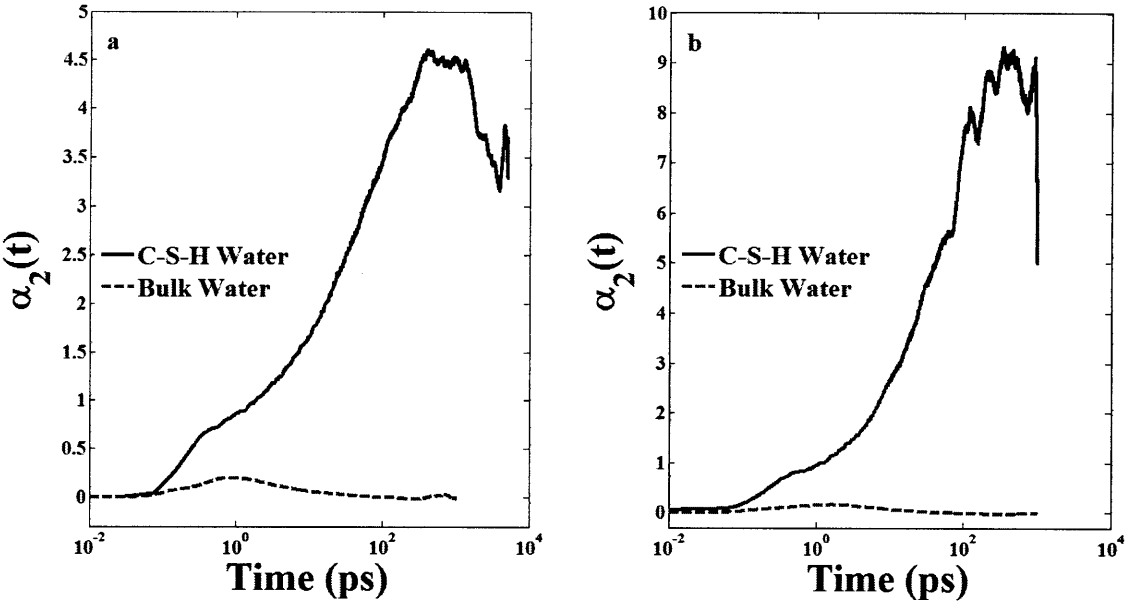

Figure 2.10 The non-Gaussian parameter $\alpha_2(t)$ calculated based on the displacement of the oxygen atom in bulk and confined water (a) using CSHFF and (b) using core-shell.

For the bulk liquid the result obtained by both potentials is in agreement with what is known from prior simulations.[48] The NGP rises to a value of less than 0.2 on a time scale $t \approx 1$ps. then it drops again to zero at the time of scale of few picoseconds. For the confined water the NGP exhibits features typical for supercooled liquids and glasses. It grows to a value of 4.5 for CSHFF and 9 for core-shell which is an order of magnitude greater than the bulk case. The growth stops and a maximum is reached at about 400 ps ending a stage known as β-relaxation. The large magnitude of the NGP in this time regime suggests that the translational dynamics of the confined water molecules is highly heterogeneous. The β-relaxation stage is followed by a slow drop of the NGP starting another stage known as α-relaxation that corresponds to the onset of the diffusive motion, consistent with our MSD results. In the hydrodynamic limit, $t \to \infty$, the NGP should decay to zero reflecting the ergodicity of the system. It is very probable that the

convergence of the NGP to zero cannot be captured in a reasonable simulation time using MD for the C-S-H system. Thus we believe that exploring the longer time scale evolution of the water confined in C-S-H requires a special treatment. An activation-relaxation based method that has been recently developed [74,75] to tackle long time scale phenomena[76,77] by following the evolution of atomic trajectories through the potential energy landscape is a potential method for future studies of the confined water dynamics in C-S-H. Overall, the stages described for the NGP, particularly the β-relaxation stage followed the α-relaxation stage is consistent with the cage to diffusive motion exhibited in the MSD results.

The glassy dynamics similar to that of a supercooled liquid exhibited by the confined water in C-S-H, particularly the cage effect in the MSD, can be explained in terms of two mechanisms. The first is the enhancement of the interstitial molecule peak. This enhancement means that there are no vacant sites in the first shell around the water molecule. This, in turn, forbids large displacements and local rearrangements can occur only through highly correlated motion of many particles. Such local rearrangements occur in domains which are temporarily more fluidized than the background.[8384] The second is that this confined water behaves as if it is effectively at a lower temperature than the true temperature. The idea of "lower effective temperature" constraining the dynamics and forming a cage stage for water confined between the hydrophilic walls was suggested previously using neutron diffraction experiments.[27] Similarly Gallo et al.[28] observed that water molecules residing close to the hydrophilic surface behaved as if they were already below the mode coupling crossover temperature when confined in a large (4 nm) nano-pore although the MD simulation was conducted at room temperature.

Therefore, we think that this dynamic constraint forming a cage stage in the MSD of water ultra-confined in C-S-H at room temperature is imposed because of the attractive interactions of water molecules with the calcium-silicate walls. We also believe that the second mechanism is more dominant in determining the glassy dynamics of this confined water since it is known for supercooled water that the cage effect is not a consequence of an increase in density but rather due to the increase of the hydrogen bond stiffness which makes the cage more rigid.[85] Such strong hydrogen bonds are formed between the confined water molecules and the non-bridging oxygen atoms in the calcium-silicate layers.

2.4 Conclusion

Controlling the macroscopic properties of a wide class of materials of important applications such as zeolites, clays and cement requires fundamental understanding of the water confined in the nano-pores of these materials. In this chapter, we studied by means of molecular simulations the water confined in the quasi two-dimensional pores of width less than 1 nm of calcium-silicate-hydrate which is the major binding phase in cement. We conducted the study using two different force fields. CSHFF incorporates a flexible non-polarizable water model, while core-shell represents water by a flexible and polarizable model. Our results indicated that a well-parameterized flexible water potential such as that in CSHFF is sufficient to capture the confinement and ion solvation effects qualitatively.

Both the interlayer calcium and the defective silicate chains in C-S-H render a hydrophilic interaction between the confined water and C-S-H. The defective silicate

chains offer acceptor hydrogen bonding sites to the confined water molecules mainly through the non-bridging oxygen atoms on the silicate layers. The interlayer calcium, as a divalent cation, facilitates the sorption of the water molecules in the interlayer space, enhancing the hydrophilicity on the interface region. The overall hydrophilic nature of this confining interface increases the polarity of the water molecules, quantified as an upshift of the water dipole moment distribution.

The confined water in C-S-H adopts a multi-component spatial structure. Each component manifests itself on a distinct length scale. At short distances (~ 2.7 Å) the tetrahedral coordination of water molecules is still preserved. At an intermediate range (up to ~4.2 Å), the triplet correlations of the oxygen-oxygen-oxygen angle distributions demonstrated that the confined water adopts a structure similar to that of dense fluids and supercooled phases. At larger distances (up to ~ 10 Å), orientational correlations persists through directional hydrogen bonds to the substrate, as evidenced through the dipole-dipole interactions between water molecules.

The intermediate range structure provided us the evidence that the confined water can behave dynamically as a glassy material. By examining the mean square displacement and the non-Gaussian parameter, we showed that the water ultra-confined by the hydrophilic interfaces of C-S-H exhibits a three-stage dynamics, with a clear "cage" stage characteristic of glassy dynamics. We think that this is induced because of the attractive interactions of water molecules with the calcium-silicate walls, serving to dynamically constrain the motion of water molecules at the interface. This was priorly interpreted as an effective temperature in water lower than the actual simulation temperature. Eventually we concluded that this confined water system stands on equal

footing with systems of slow heterogeneous dynamics such as supercooled liquids and glasses.

2.5 References

1. Eisenberg, D.; Kauzmann, W. *The Structure and Properties of Water*; Oxford University Press: New York, 1969.
2. Mentre, P. *Cell. Mol. Biol.* **2001**, *47*, 709.
3. Karaborni, S.; Smit, B.; Heidug, W.; Urai, J.; van Oort, E. *Science* **1996**, *271*, 1102.
4. Puibasset, J.; Pellenq, R. *J. Phys. Chem. B* **2008**, *112*, 6390.
5. Bordallo, H.; Aldridge, L.; Desmedt, A. *J. Phys. Chem. B* **2006**, *110*, 17966.
6. Chen, S.-H.; Mallamace, F.; Mou, C.-Y.; Broccio, M.; Corsaro, C.; Faraone, A; Liu, L. *Proc. Natl. Acad. Sci. U.S.A.* **2006**, *103*, 12974.
7. Bergman, R.; Swenson, J. *Nature* **2000**, *403*, 283.
8. Major, R.; Houston, J.; McGrath, M.; Siepmann, J.; Zhu, X.-Y. *Phys. Rev. Lett.* **2006**, *96*, 177803.
9. Raviv, U.; Laurat, P.; Klein, J. *Nature* **2001**, *413*, 51.
10. Taylor, H. F. W. *Cement Chemistry*, 2nd ed.; Thomas Telford: London, 1997.
11. Allen, A.; Thomas, J.; Jennings, H. *Nature Materials* **2007**, *6*, 311.
12. Pellenq, R.; Kushima, A.; Shahsavari, R.; Van Vliet, K.; Buehler, M.; Yip, S.; Ulm, F.-J. *Proc. Natl. Acad. Sci. U.S.A.* **2009**, *106*, 16102.
13. Ridi, F.; Luciani P.; Fartini, E.; Baglioni, P. *J. Phys. Chem. B* **2009**, *113*, 3080.
14. Jönsson, B.; Wennerström; Nonat, A.; Cabane, B. *Langmuir* **2004**, *20*, 6702.
15. Vandamme, M.; Ulm, F.-J. *Proc. Natl. Acad. Sci. U.S.A.* **2009**, *106*, 10552.
16. Mindess, S.; Young, J. F. *Concrete*, Prentice Hall: Englewood Cliffs, NJ, 1981.
17. Neville A. M. *Properties of Concrete*, 4th ed.; Prentice Hall: Upper Saddle River, NJ, 1995.
18. Sposito, G.; Prost, R. *Chem. Rev.* **1982**, *82*, 553.
19. Dick, A.; Overhauser, B. *Phys. Rev.* **1958**, *112*, 90.
20. Shahsavari, R.; Pellenq, R.; Ulm, F.-J. *Langmuir,* (submitted, in review).

21. Cicero, G.; Grossman, J.; Schwegler, E.; Gygi, F.; Galli, G. *J. Am. Chem. Soc.* **2008**, *130*, 1871.

22. van Maaren, P.; van der Spoel, D. *J. Phys. Chem. B* **2001**, *105*, 2618.

23. Smirnov, K.; Bougeard, D. *Chemical Physics* **2003**, *292*, 53.

24. Berendsen, H.; Grigera, J.; Straatsma, T.; *J. Phys. Chem.* **1987**, *91*, 6269.

25. van Buuren, A.; Marrink, S.; Berendsen, H. *J. Phys. Chem.* **1993**, *97*, 9206.

26. Teleman, O.; Jonsson, B.; Engstrom, S. *Mol. Phys.* **1987**, *60*, 193.

27. Dore, J. in *Correlations and connectivity* (Eds Stanley, E. H.; Ostrowsky, N.) ; Kulwer Academic: Dordrecht, 1990.

28. Gallo, P.; Rovere, M.; Spohr, E. *Phys. Rev. Lett.* **2000**, *85*, 4317.

29. Lewis, G.; Catlow, C. *J. Phys. C: Solid State Phys.* **1985**, *18*, 1149.

30. Kundu, T.; Rao, H.; Parker, S. *J. Phys. Chem. B* **2005**, *109*, 11286.

31. Kerisit, S.; Ilton, E.; Parker, S. *J. Phys. Chem. B* **2006**, *110*, 20491.

32. Kerisit, S.; Cooke, D.; Spagnoli, D.; Parker, S. *J. Mater. Chem.* **2005**, *15*, 1454.

33. Spagnoli, D.; Cooke, D.; Kerisit, S.; Parker, S. *J. Mater. Chem.* **2006**, *16*, 1997.

34. de Leeuw, N.; Parker, S. *Phys. Rev. B* **1998**, *58*, 13901.

35. Kerisit, S.; Parker, S. *J. Am. Chem. Soc.* **2004**, *126*, 10152.

36. Allen, M.; Tildesley, D. *Computer Simulation of Liquids*, Oxford University Press: New York, 1987.

37. Gale, J. *J. Chem. Soc. Faraday Trans.* **1997**, *93*, 629.

38. Gale, J. *Phil. Mag. B* **1996**, *73*, 3.

39. Gale, J.; Rohl, A. *Mol. Simul.* **2003**, 29, 291.

40. Shanno, D. *Math. Comp.* **1970**, *24*, 647.

41. Banerjee, A.; Adams, N.; Simons, J.; Shepard, R. *J. Phys. Chem.* **1985**, *89*, 52.

42. Smith, W.; Yong, C.; Rodger, P. *Mol. Simul.* **2002**, *28*, 385.

43. Smith, W. *Mol. Simul.* **2006**, *32*, 933.

44. Mitchell, P.; Fincham, D. *J. Phys.: Condens. Matter.* **1993**, *5*, 1031.

45. Park, S.-H.; Sposito, G. *J. Phys. Chem. B* **2000**, *104*, 4642.

46. Soper, A.K.; Phillips, M. G. *Chem. Phys.* **1986**, *107*, 47.

47. Chaudhuri, P.; Berthier, L. ; Kob, W. *Phys. Rev. Lett.* **2007**, *99*, 060604.

48. Caprion, D.; Matsui, J.; Schober, H. R. *Phys. Rev. Lett.* **2000**, *85*, 4293.

49. Ricci, M. A.; Bruni, F.; Giuliani, A. *Faraday Discuss.* **2009**, *141*, 347.

50. Strassle, T.; Saitta, A. M.; Godec, Y. L.; Hamel, G.; Klotz, S.; Loveday, J. S.; Nelmes, R. J. *Phys. Rev. Lett.* **2006**, *96*, 067801.

51. Di Cicco, A; Trapananti, A; Faggioni, S *Phys. Rev. Lett.* **2003**, *91*, 135505.

52. Shirono, K.; Daiguji, H. *Chem. Phys. Lett.* **2006**, *417*, 251.

53. Stöckelman E.; Hentschke, R. *J. Chem. Phys.* **1999**, *110*, 12097.

54. Marx, D.; Spirk, M.; Parrinello, M., *Chem. Phys. Lett.* **1997**, *273*, 360.

55. Lightstone, F. C.; Schwegler, E.; Allesch, M.; Gygi, F.; Galli, G. *ChemPhysChem* **2005**, *6*, 1745.

56. Bako, I.; Hutter, J.; Palinkas, G. *J. Chem Phys.* **2002**, *117*, 9838.

57. Churakov, S. V. *Am. Mineral.* **2009**, *94*, 156.

58. Ockwig, N. W.; Greathouse, J. A.; Durkin, J. S.; Cygan, R. T.; Daemen, L. L.; Nenoff, T. M. *J. Am. Chem. Soc.* **2009**, *131*, 8155.

59. Greenwell, H. C.; Jones, W.; Coveney, P. V.; Stackhouse, S. *J. Mater. Chem.* **2006**, *16*, 708.

60. Dokter, A. M.; Woutersen, S.; Bakker, H. J. *Proc. Natl. Acad. Sci. U.S.A.* **2006**, *103*, 15355.

61. Badyal, Y. S.; Saboungi, M. -L.; Price, D. L.; Shastri, S. D.; Haeffner, D. R.; Soper, A. K. *J. Chem. Phys.* **2000**, *112*, 9206.

62. Nymand, T. M.; Linse, P. *J. Chem. Phys.* **2000**, *112*, 6386.

63. Rahman, A. *Phys. Rev.* **1964**, *136*, A405.

64. Kob, W. *J. Phys.: Condens. Matter* **1999**, 11, R85.

65. Roder, A.; Kob, W.; Binder, K. *J. Chem. Phys.* **2001**, *114*, 7602.

66. Kete, S.; Xu, Z.; Ihle, B.; Buehler, M. J. *Nature Materials* **2010**, *9*, 359.

67. Hu, M.; Goicochea, J. V.; Michel, B.; Poulikakos, D. *Nano Lett.* **2010**, *10*, 279.

68. Baruah, B.; Roden, J. M.; Sedgwick, M.; Correa, M.; Crans, D. C.; Levinger, N. E. *J. Am. Chem. Soc.* **2006,** *128*, 12758.

69. Coudert, F.-X.; Vuilleumier, R.; Boutin, A. *ChemPhysChem* **2006**, *7*, 2464.

70. Dyer, P. J.; Cummings, P. T. *J. Chem. Phys.* **2006**, *125*, 144519.

71. Kagel, W. K.; van Blaaderen, A. *Science* **2000**, *287*, 290.

72. Weeks, E. R.; Crocker, J C.; Levitt, A. C.; Chobfield, A.; Weitz, D. A. *Science* **2000**, *287*, 627.

73. Hurley, M. M.; Harrowell, P. *J. Chem. Phys.* **1996**, *105*, 10521.

74. Kushima, A.; Lin, X.; Li, J.; Eapen, J.; Mauro, J. C.; Qian, X.; Diep, P.; Yip, S. *J. Chem. Phys.* **2009**, *130*, 224504.

75. Kushima, A.; Lin, X.; Li, J.; Eapen, J.; Mauro, J. C.; Qian, X.; Diep, P.; Yip, S. *J. Chem. Phys.* **2009**, *131*, 164505.

76. Lau, T. T.; Kushima, A.; Yip, S. *Phys. Rev. Lett.* **2010**, *104*, 175501.

77. Fan, Y.; Kushima, A.; Yildiz, B. *Phys. Rev. B* **2010**, *81*, 104102.

78. Ockwig, N. W.; Greathouse, J. A.; Durkin, J. S.; Cygan, R. T.; Daemen, L. L.; Nenoff, T. M. *J. Am. Chem. Soc.* **2009**, *131*, 8155.

79. Nakanishi, M.; Nozaki, R. *Phys. Rev. E* **2010**, *81*, 041501.

80. Crauste-Thibierge, C.; Brun, C.; Ladieu, F.; L'Hote, D.; Biroli, G.; Bouchaud, J-P. *Phys. Rev. Lett.* **2010**, *104*, 165703.

81. Cicero, G.; Grossman, J. C.; Catellani, A.; Galli, G. *J. Am. Chem. Soc.* **2005**, *127*, 6830.

82. Boon, J. P.; Yip, S. *Molecular Hydrodynamics*, Dover: New York, 1991.

83. Adam, G.; Gibbs, J. H. *J. Chem. Phys.* **1965**, *43*, 139.

84. Zangi, R.; Rice, S. A. *Phys. Rev. E*, **2003**, *68*, 061508.

85. Gallo, P.; Rovere, M.; Spohr, E. *J. Chem. Phys.* **2000**, *113*, 11324.

86. Bellissent-Funel, M.-C. *J. Mol. Liq.* **1998**, *78*, 19.

87. Lombardo, T. G.; Giovambattista N.; Debenedetti, P. G. *Faraday Discuss.* **2009**, *141*, 359.

Chapter 3: Cationic Exchange in Calcium-Silicate-Hydrate. The Case Study of Strontium-90 ($^{90}Sr^{2+}$)

3.1 Concrete, Cement and C-S-H in the Near Field of the Disposed Radioactive Waste

The management and disposal of radioactive waste from the use of radionuclides in industry and medicine, radioisotope production facilities, fuel processing plants and the spent nuclear fuel is a major challenge. The latter source of radioactivity, the spent nuclear fuel, is the longest-lived, the most highly radioactive and the most challenging type of waste. In most countries the preferred technological approach is the disposal of the radioactive waste in repositories constructed in rock formations hundreds of meters below the earth's surface.[1]

Historically there were concerns associated with the use of cementitious materials in radioactive waste repositories.[11] The primary concern is the presence of portlandite ($Ca(OH)_2$) in these materials which is highly soluble when it comes into contact with ground water. Upon dissolution, portlandite raises the pH in the pore water of cement to values greater than 11. This high pH environment is ideal for facilitating the mobility and migration of the radionuclides to the far field. Currently the accepted solution to this issue is developing cementitious materials that generate pore water with pH <11. This is equivalent to reducing the amount of portlandite. Typically this is achieved by adding pozzolanic minerals with high silica content such as silica fume and fly ashes to the blend of cement. The pozzolanic (glassy) silica consumes portlandite and produces C-S-H.[34]

Low-pH cementitious materials can be used for different purposes in the near field of the radioactive waste repository. For example, they can be used as a shielded cask to protect the waste package, as grouting for sealing cracks in the repository, as liners for the repository tunnels or most importantly as the inner most waste form itself.[12,6] As a waste form, the cement matrix is capable of immobilizing a myriad of radionuclides. However, the mechanism of immobilization is very species sensitive[7] which implies that an effort has to be devoted to understand the interaction of each radionuclide with the cement matrix. In spite of this, it is possible to state that in general C-S-H is particularly relevant for the uptake of metal cations, whereas other minor phases such as Ettringite (see chapter 1), can potentially immobilize anions.[12]

Cation exchange is regarded as one of the key processes that regulate the uptake of metal cations in C-S-H.[789] The immobilization by cation exchange is not limited to the disordered C-S-H in actual cement paste, but it can also take place in a crystalline family of C-S-H which is tobermorite.[1011,12] Since it is thermodynamically favorable to incorporate tobermorite in cement and concrete,[11] it was suggested to use them to extract the radioactive metal cation first and then blend them with cements. In this study we consider the cationic exchange as a mechanism for radioactive metal cations immobilization in both the disordered C-S-H and a member of the tombermorite family which is tobermorite 9 Å. Demonstrating the capability to engineer cementations materials at the atomistic level to capture radionuclides is an essential step forward in progressing in this area. In the next section we introduce the metal cation of interest.

3.2 Strontium-90 ($^{90}Sr^{2+}$)

We consider the spent nuclear fuel as it is the most challenging source of radioactivity. At different times, different radionuclides are the dominant contributors to the overall radioactivity, radiotoxicity and decay heat emitted by the fuel.[1] Figure 3.1 depicts the radioactivity profile of spent nuclear fuel discharged from a pressurized water

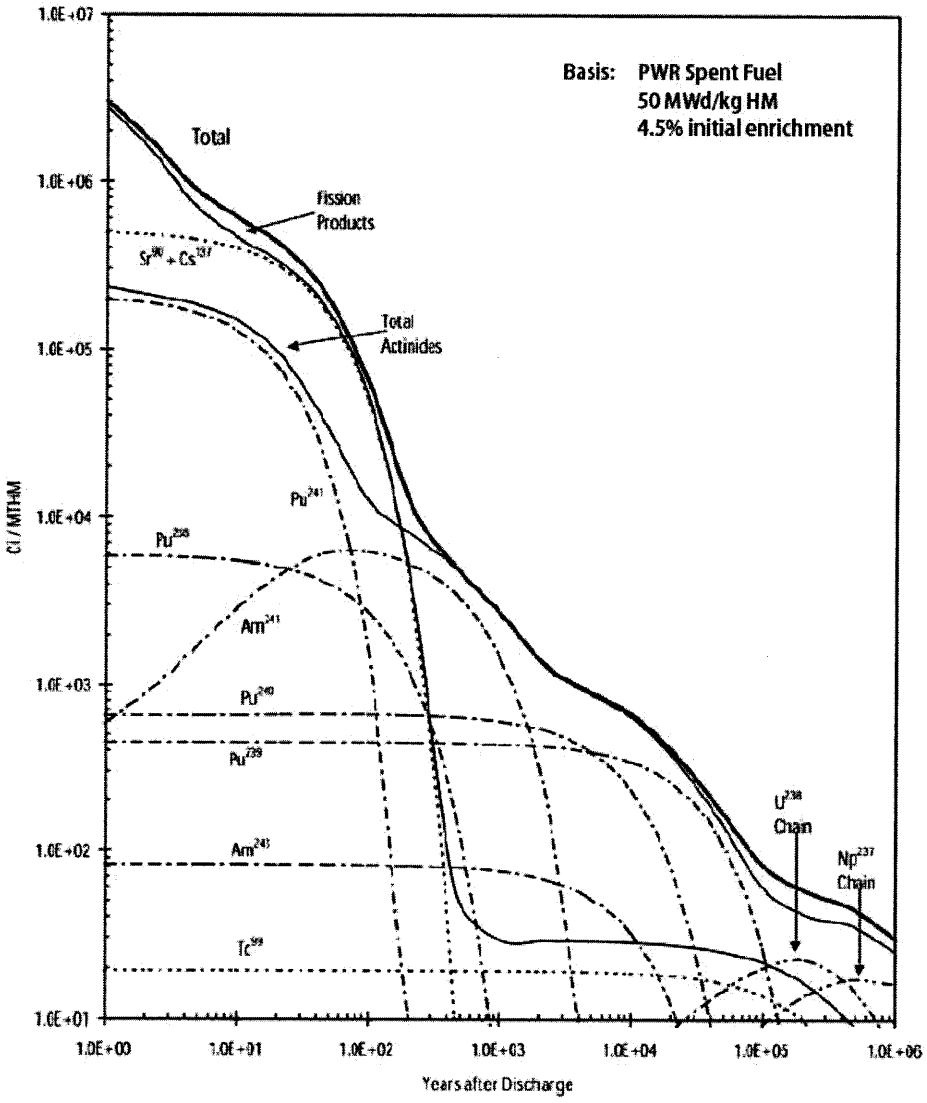

Figure 3.1 Radioactivity profile of spent fuel as a function of time after discharge.[1]Radioactivity unit is Curie per megaton of heavy metal (Ci/MTHM).

reactor (PWR) assuming a burn up rate of 50 MWd/kg HM[†] and an initial enrichment of 4.5%. It is evident from the figure that the two fission products strontium-90 ($^{90}Sr^{2+}$) and cesium-137 ($^{137}Cs^{+}$) account for the bulk radioactivity for the next several decades after discharge. Thereafter, the actinides become the dominant contributors to the radioactivity. Therefore it is more urgent at this stage to understand the immobilization mechanism of $^{90}Sr^{2+}$ and $^{137}Cs^{+}$ and to evaluate the integrity of a waste form that encapsulate these radionuclides.

In this thesis we focus on encapsulating $^{90}Sr^{2+}$ in the disordered C-S-H and tobermorite 9Å. It is known that the cation exchange $Sr^{2+} \leftrightarrow Ca^{2+}$ is the mechanism of immobilizing $^{90}Sr^{2+}$ in C-S-H[7,813] and tobermorite.[14,15] In fact it was shown that tobermorite exhibits partial to complete exchange of Ca^{2+} for divalent cations.[14] However, the exchange sites, and the effect on the stability and mechanical integrity of the waste form are uncertain. It is our goal to shed some light on these uncertainties in this study by means of atomistic simulations. In the next section we describe the computational approach to this problem and the rest of the chapter is a discussion for the obtained results.

3.3 Computational Approach

3.3.1 Molecular Models

For the disordered C-S-H we used the same model described previously in chapter 1 and 2. We realize that the Ca/Si for this model is 1.65 which is high for radioactive waste confinement applications. The addition of glassy silica to the low-pH cement

[†] Megawatt day per kilogram of heavy metal.

results in the formation of C-S-H whose Ca/Si is less than 1.2. [16] However, at the time of conducting this study, the above mentioned model was the only available one for C-S-H. We regard this study as the first step in studying the cationic exchange in the disordered C-S-H. In the future when there are models for C-S-H with lower Ca/Si available, we can perform a similar work on them.

The triclinic structure of tobermorite 9Å resolved by Merlino et al.[17] is our model to represent this mineral. It has layered structure with infinite silicate chains similar to the whole family of tobermorite. However, the calcium-silicate layers are closer to each other (compared to other members of the family) and the mineral is completely dehydrated except from hydroxyl groups attached to silicon atoms. The very narrow channels between the calcium-silicate layers hosts only interlayer calcium. Figure 3.2 is a depiction for 4 unit cells of this mineral and Table 3.1 is a comparison between the disordered C-S- H and the tobermorite under consideration.

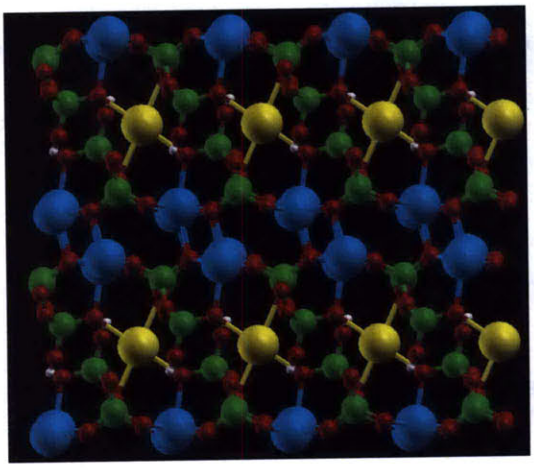

Figure 3.2 Merlino structure for tobermorite 9 Å. White spheres are hydrogen atoms, red are oxygen, green are silicon, light blue are layer calcium and yellow are interlayer calcium.

Table 3.1 Comparison between the disordered C-S-H and tobermorite 9Å.

	Disordered C-S-H	Tobermorite 9Å
Chemical Formula	$(CaO)_{1.65}$-(SiO_2)-$(H_2O)_{1.73}$	$Ca_5Si_6O_{16}.(OH)_2$
Ca/Si	1.65	0.83
H/Si[a]	1.73	0.17
Cw/Ca_poly[b]	0.55	0.25
Density (g/cm^3)[c]	2.50	2.66
Number of unit cells used in the simulations	Two sheets	2×3×2

a Strictly speaking this should be the water-to-silicon ratio. Here we count each two hydrogen atom as if they belong to a dissociated water molecule.

b This is the ratio between the interlayer calcium denoted by Cw and the layer (polyhedral sheets) calcium denoted by Ca_poly.

c Calculated densities.

3.3.2 Force Field

The core-shell force field described in chapter two is used to perform the simulations for the cationic exchange problem. The strontium-water potential was derived by Kerisit and Parker,[35] while strontium-layer oxygen potential is based on the work of Lewis and Catlow.[19] The strontium-layer oxygen potential was successfully used in modeling cationic exchange in zeolites.[20] Finally, we derived the strontium-hydroxyl potential form the strontium-layer oxygen potential by standard mixing rules.[‡] All the parameters are given in appendix B.

[‡] The Buckingham parameter (ρ) is kept fixed and the parameter (A) is scaled to the charges.

As a first test for the core-shell force field in modeling tobermorite 9Å, we compared the structure predicted by structure optimization and by isobaric-isothermal (NPT) molecular dynamics (MD)[§] with the experimentally determined structure by Merlino et al.[17] Table 3.2 summarizes the comparison and the relative error.

Table 3.2 Comparison of the structural properties of tobermorite 9Å derived from structure optimization and NPT-MD with the experimentally determined structure.

	Experimental	**Structure Optimization**		**NPT-MD**	
		value	error %	value	error %
***a* axis (Å)**	11.156	11.255	0.89	11.250	0.84
***b* axis (Å)**	7.303	7.312	0.90	7.275	-0.38
***c* axis (Å)**	9.566	10.096	5.54	10.553	10.32
***α* angle (deg)**	101.08	96.97	-4.06	98.62	-2.43
***β* angle (deg)**	92.83	88.12	-5.07	88.04	-5.16
***γ* angle (deg)**	89.98	89.30	-0.76	89.26	-0.80

Although the *c* axis that is perpendicular to the calcium-silicate layers is overestimated , we regard the agreement between the calculated and the experimental results good given that this force field was not fitted to the family of tobermorite.

[§] *T= 300* K, *P= 0* GPa

3.3.3 Structure Optimization and Molecular Dynamics

As in chapter 2, the purpose of structure optimization is achieving a reasonable structure that is consequently used in the finite temperature molecular dynamics. However, we extended the role of structure optimization here to determine the energetically favorable site for the cationic exchange $Sr^{2+} \leftrightarrow Ca^{2+}$ and the mechanical properties of the cementitious waste form as a function of strontium concentration $[Sr^{2+}]$. To perform this we distinguished between two Ca^{2+} cation sites in the bulk structure of C-S-H and tobermorite 9Å, i.e., the interlayer site and the polyhedral sheet site. To simulate the cation exchange in the interlayer sites, a Ca^{2+} cation in the interlayer space is chosen at random and replaced by Sr^{2+}, then the structure is optimized by allowing an all-atoms relaxations and simulation cell volume and shape relaxation. Upon full relaxation the elastic constants matrix is calculated, from which the bulk, shear and indentation moduli are calculated. This process is repeated until all the interlayer sites are exchanged. The same method was applied to the polyhedral sheet sites but we stopped the exchange when a number of sites equal to the interlayer sites are exchanged. We did not fully exchange all the polyhedral sheets sites to provide a basis for the comparison between the two sites under consideration. We used the code General Utility Lattice Program (GULP) to perform these simulations.

We performed six molecular dynamics simulations (MD) to study the structure stability of the strontium-substituted cementitious waste form and the coordination of the immobilized strontium. Two simulations were performed for the pure C-S-H and tobermorite 9Å, two simulations when all of the interlayer sites are substituted, and finally two simulations when all the polyhedral sites are substituted. In all cases we

performed 250 ps of equilibration in the isobaric-isothermal ensemble (NPT) at a pressure of 0 GPa and a temperature of 300 K. During these simulations, configurations with cell vectors close to the average equilibrium values were taken and used to start canonical ensemble (NVT) simulations. The production simulations in the NVT ensemble were 200 ps long. The code DL_POLY_2 was used to perform all MD simulations and the rest of simulation details were explained in chapter 2.

3.4 Results and Discussion

This section is a discussion of the insights gained from performing the simulations described above. It is divided into three subsections. In the first subsection we deduce the energetically favorable exchange sites based on the potential energy considerations. In the second part, we discuss the stability of the waste form and the coordination environment of the bound strontium cation. Finally, in the last section we evaluate the mechanical integrity of the waste form based on the calculation of the elastic moduli.

3.4.1 Energetically Favorable Exchange Sites

We calculated the potential energy of C-S-H and tobermorite 9Å as a function of strontium substitution both in the interlayer sites and the polyhedral sites. The potential energy is used here as a metric to determine the favorable exchange site. Figure 3.3 shows the results for both phases and for the two sites under consideration. In the case of C-S-H the substitution in the interlayer space is only slightly favorable at high substitution concentrations. At low concentration there is almost no distinction between them. This explains why it was difficult to determine by experiments which site is favorable, because in these experiments C-S-H is doped by a very low concentration of

strontium.[813] and at very low concentrations, both sites seems to be equally favorable. On the other hand for tobermorite 9Å, it is clear that the substitution in the interlayer space is more favorable energetically compared to the polyhedral sheets substitution at all concentrations.

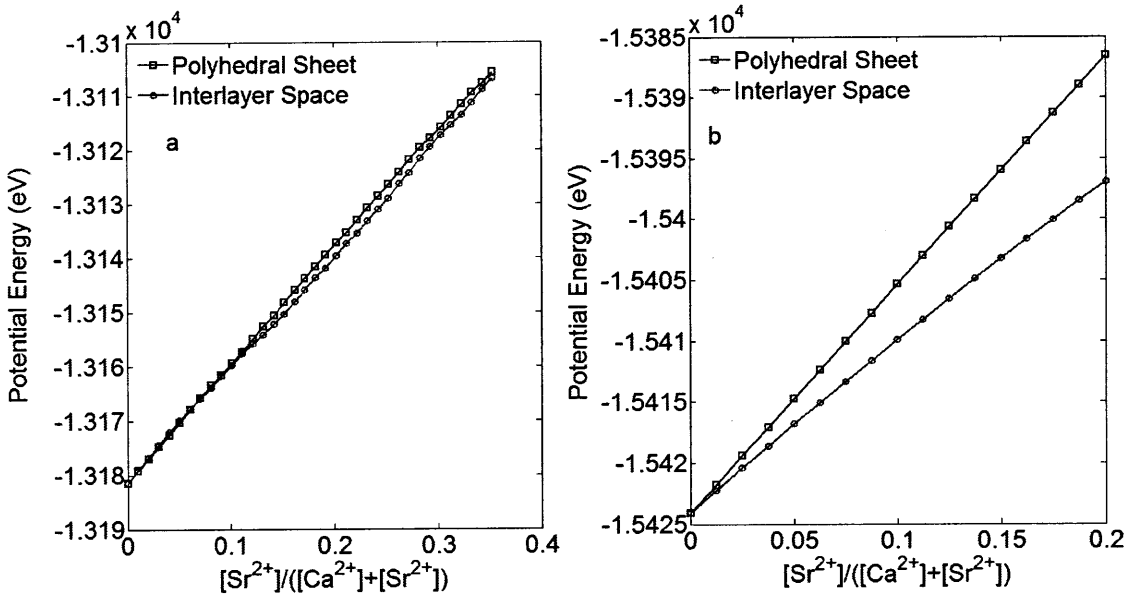

Figure 3.3 The potential energy of C-S-H (a) and tobermorite 9Å (b) as a function of strontium substitution in the interlayer space sites and the polyhedral sheets sites.

3.4.2 Structural Stability and the Binding Environment

We used our finite temperature molecular dynamics simulations to assess the stability of the structure of the waste forms under consideration. Our specific metric in this context is the stability of the silicate chains grafted on the layers upon strontium substitution. The choice of this metric is based on an experimental study for the encapsulation of cesium (Cs^+) by C-S-H. [21] In this study it was shown that Cs^+ breaks the silicate chains of C-S-H.

In our simulations we know the proportions of the different types** of the silica tetrahedra in the pure C-S-H and tobermorite 9Å. For C-S-H these proportions are Q^0 ~10 %, Q^1 ~ 67% and Q^2 ~ 23%, while for tobermorite 9Å there is only Q^2 as the silicate chains in this well-crystallized mineral are infinite in length. Full strontium substitution in the interlayer space or in the polyhedral sheet does not change these proportions of the silica tetrahedra in both waste forms within the simulation time considered. This result shows that the structure of both waste forms is stable. Figure 3.3 demonstrates the stability of the silicate chains for the pure case, full substitution in the interlayer space and full substitution in the polyhedral sheet.

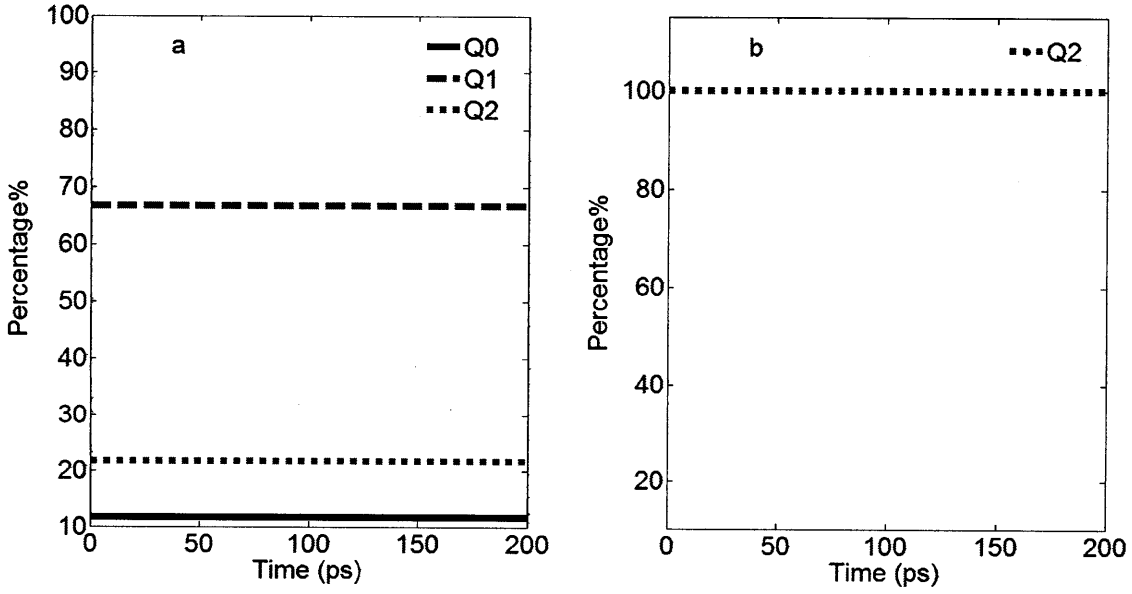

Figure 3.4 The proportions of the silica tetrahedra in C-S-H (a) and tobermorite 9Å (b) as a function of simulation time. These proportions are the same for the simulation of the pure materials, when the interlayer calcium is fully substituted by strontium and when all the polyhedral calcium is fully substituted by strontium.

** See Section 1.2 for a definition of the types of the silica tetrahedra.

After demonstrating the stability of the structure of the waste forms we turn to discuss the coordination of the bound strontium cation Sr^{2+}. We characterize the coordination of the bound cation in terms of bond lengths and coordination numbers in the first shell. In particular we calculated both the Sr-O bond length and the Sr-Si distance from the position of the first peak of the corresponding radial distributing functions. The coordination numbers for O and Si in the first shell around Sr were calculated using equation (2.1). These parameters can also be extracted from Extended X-ray Absorption Fine Structure (EXAFS) experiments. In Table 3.3 we summarize the results obtained from our molecular dynamics simulations accompanied with the results obtained from EXAFS experiments performed on Sr-doped C-S-H.[13]

Table 3.3 A summary for bond lengths and the corresponding coordination numbers (N) around the bound strontium. The experimental results are taken from reference 13.

	T(K)	Ca/Si (initially)	H/S	Sr-O (Å)	N	Sr-Si (Å)	N
C-S-H/ Interlayer	300	1.65	1.73	2.52	6.68	3.67	3.1
C-S-H/Polyhedral	300	1.65	1.73	2.50	6.62	3.65	4.2
Tobermorite/ Interlayer	300	0.83	0.17	2.49	4.24	3.64	6.2
Tobermorite/ Polyhedral	300	0.83	0.17	2.49	7.08	3.64	5.5

C-S-H (Exp)	77	0.7	-	2.60	6.3	-	-
C-S-H (Exp)	77	1.1	-	2.61	7.6	4.33	2.0

The differences between the experiments and the simulations both in temperature and in chemistry do not allow direct comparison between them. However, we regard our results here as a demonstration that it is possible ,in principle, to validate our computational models through EXAFS experiments by unifying the conditions under which simulations and experiments are conducted. Accomplishing this, will render our computational models a powerful predictive tool.

3.4.3 The Mechanical Integrity of the Waste Form

Finally we assess the durability of the waste forms based on their mechanical integrity after the cationic exchange had taken place. For that purpose we calculated the bulk, shear and indentation moduli as a function of strontium substitution. These moduli contain information about the response of the waste form to various types of deformation. Shear (G) and bulk (K) moduli were calculated using Hill convention[22] while the indentation modulus (M) was determined by the relationship:[23]

$$M = 4G\frac{3K+G}{3K+4G} \qquad (3.1)$$

Experimentally it is possible to measure a statistically significant indentation modulus for C-S-H by the grid indentation technique,[24] which makes our results regarding the mechanical integrity amenable to validation as well. Figure 3.5 shows the obtained results for both C-S-H and tobermorite 9Å.

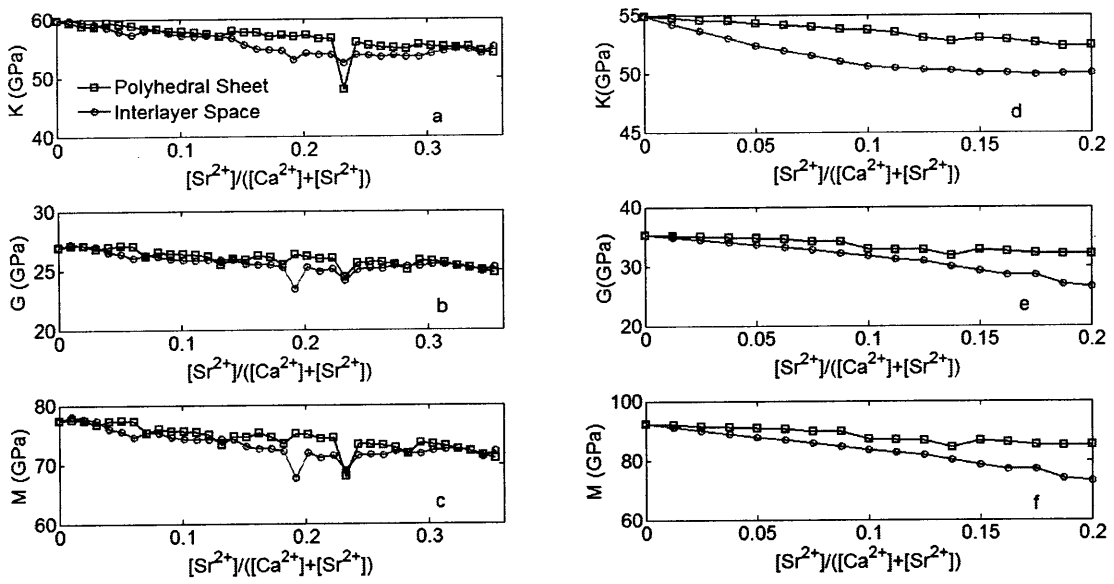

Figure 3.5 The mechanical properties of the waste forms as a function of strontium substitution. (a), (b) and (c) are the bulk, shear and indentation moduli of C-S-H, respectively. (d), (e) and (f) are the bulk, shear and indentation moduli of tobermorite 9Å, respectively. The legend applies to all plots.

In general the mechanical properties degrade as the strontium concentration increases. The substitution in the interlayer space, which is energetically favorable, degrades the mechanical properties more than the substitution in the polyhedral sheet. This trend is more pronounced in tobermorite 9Å. It is expected that substitution in the interlayer space weakens the material more compared to the polyhedral sheet since these layered materials are generally weak in the interlayer direction and in addition to this the ionic radius of strontium is larger than that of calcium. The consequence is that the substitution increases the thickness of the interlayer space which is the weakest direction. In spite of this, we believe that the overall degradation in these waste forms is not limiting and does not exclude cementitious materials as potential waste forms.

3.5 Concluding Remarks

In this chapter we explored the potential use of two members of the calcium-silicate-hydrate family, disordered C-S-H and tobermorite 9Å, as waste forms to immobilize the radionuclide strontium-90 ($^{90}Sr^{2+}$) by means of atomistic simulations. Our results showed that the cationic exchange $Sr^{2+} \leftrightarrow Ca^{2+}$ is energetically favorable to take place in the interlayer space. Furthermore this exchange does not affect the stability of the silicate chains in both waste forms. Finally we showed that the mechanical properties degrade as strontium concentration increases in the waste form, however, we believe that this degradation is not limiting.

Several studies[15,25] showed that Aluminum-substituted C-S-H and tobermorite have more capacity to immobilize metal cations compared to the pure phases. In future studies we can consider Aluminum-substituted phases as our starting models. Moreover, it was shown recently by Mandaliev et al that Neodymium substitution in tobermorite is accompanied by a partial release of the water molecules in the interlayer space. This reflects the fact that the equilibrium hydration level can change by substituting new elements in the structure of the hydrated C-S-H phases. This can also be addressed in the future by performing grand canonical monte carlo simulations at each cationic exchange step to determine the equilibrium hydration level.

3.6 References

1. *The Future of Nuclear Power*, an interdisciplinary MIT study, 2003.
2. Forsberg, C. W.; Dole, L. *International High-Level Radioactive Waste Management Conference,* Las Vegas, 2008.
3. Saeki, T.; Monteiro, P.J.M. *Cem. Concr. Res.* 2005, *35*, 1914.

4. Dole, L.; Mattus, C. *R&D on low-pH cement for geological repository. 3rd workshop*, Paris, 2007.

5. Wiedland, E.; Johnson, C. A.; Lothenbach, B.; Winnefeld, F. *Mat. Res. Soc. Symp. Proc.* 2006, *932*.

6. Glasser, F. P. *Cem. Concr. Res.* 1992, *22*, 201.

7. Evans, N. D. M. *Cem. Concr. Res.* 2008, *38*, 543.

8. Tits, J.; Wieland, E.; Muller, C. J., Landesman, C.; Bradbury, M. H. *J. Colloid Interface Sci.* 2006, *300*, 78.

9. Mandaliev, P.; Dahn, R.; Tits, J.; Wehrli, B.; Wieland, E. *J. Colloid Interface Sci.* 2010, *342*, 1.

10. Mandaliev, P.; Wieland, E.; Dahn, R.; Tits, J.; Churakov, S. V.; Zaharako , *Applied Geochemistry* 2010, 25, 763.

11. Komarneni, S.; Roy, D. M. *Science* 1983, *221*, 647.

12. Komarneni, S.; Breval, E.; Roy, D. M.; Roy, R. *Cem. Concr. Res.* 1988, *18*, 204.

13. Wieland, E.; Tits, J.; Kunz, D.; Dahn, R. *Environ. Sci. Technol.* 2008, *42*, 403.

14. Komarneni, R.; Roy, R., Roy, D. M. *Cem. Concr. Res.* 1986, *16*, 47.

15. Ma, W.; Brwon, P. W.; Komarneni, S. *J. Am. Ceram. Soc.* 1996, *79*, 1707.

16. Alonso, M. C.; Luco, L.F.; Garcia, J. L.; Hidalgo, Huertas, F. *Proceedings of the 12th International Congress of the Chemistry of Cement*, Montreal, 2007.

17. Merlino, S.; Bonaccorsi, E.; Armbruster, T. *Am. Miner.* **1999**, *84*, 1613.

18. Kerisit, S.; Parker, S. *J. Am. Chem. Soc.* **2004**, *126*, 10152.

19. Lewis, G. V.; Catlow, C. R. A. *J. Phys. C: Solid State Phys.* **1985**, *18*, 1149.

20. Higgins, F. M.; de Leeuw, N.H.; Parker, S. C. *J. Mater. Chem.* **2002**, 12, 124.

21. Iwaida, T.; Nagasaki, S.; Tanaka, S.; Yaita, T.; Tachimori, S. *Radiochem. Acta* **2002**, *90*, 677.

22. Nye, J.F. *Physical Properties of Crystals*, Oxford University Press: New York, 1957.

23. Sneddon, I.N. *Int. J. Eng. Sci.* **1965**, *3*, 47.

24. Constantinides, G.; Ulm, F. -J. *J. Mech. Phys. Solids* **2007**, *55*, 64.

25. Tsuji, M.; Komarneni, S. *J. Mater. Res.* **1989**, *4*, 698.

Chapter 4: Epilogue and Future Work

4.1 Epilogue

In this thesis we addressed two fundamental problems in a material that has been in use by humans for thousands of years. The first problem is the nature of the water ultra-confined in hydrophilic nano-pores of thickness less than 1 nm and the second one is the cationic exchange between a radioactive metal cation and a pristine cation, both in calcium-silicate-hydrate (C-S-H) which the backbone of the cement paste. Although the original motivation for addressing these problems stemmed from the need to assess the performance of cementitious materials in the nuclear fuel cycle, it is perfectly legitimate to claim that our insights gained from the physical system under consideration is transferable to other systems of scientific and technological interest such as zeolites, clays and biological gels. Beyond the transferability, we believe that our incorporation of atomic-scale simulations is undoubtedly a new approach in cement science.

In the first problem, we demonstrated that the type of interaction between the ultra-confined water and the C-S-H substrate is hydrophilic. By careful examination of the structure of the ultra-confined water in C-S-H, we showed that it adopts a multi-range structure. At very short distances it retains a tetrahedral coordination that is slightly distorted compared to bulk water, at intermediate distances it adopts a structure similar to dense fluids and supercooled liquids and at long ranges the water molecules are still correlated through dipole-dipole interaction that originates from the directionality of the hydrogen bonding to the substrate. Finally by exploring the translational dynamics of this confined water, we demonstrated that it is in a glassy state as if the confined water is at

an effective temperature lower than the room temperature at which the simulations were performed. This glassy state of the confined water was shown to be dynamically heterogeneous and was attributed to the attractive interaction between the water molecules and the hydrophilic walls of C-S-H. These findings on the microscopic structure and dynamics of water confined in C-S-H have important implications on describing the cohesion and mechanical behavior of cement from its setting to its aging.

In the second problem, we deduced that the interlayer sites are the energetically favorable ones for the cationic exchange $Sr^{2+} \leftrightarrow Ca^{2+}$ to take place in C-S-H and tobermorite 9 Å with the trend more pronounced in the latter. The structure of the cementitious waste from was shown to be stable upon strontium substitution. Furthermore, we observed a degradation in the mechanical properties of the cementitious waste from when strontium substitutes calcium, however, we believe that this degradation is not severe and hence does not limit the use of cement as a waste form for strontium.

4.2 Future Work

In this thesis we examined the properties of confined water in C-S-H at Ca/Si of 1.65 and H/Si of 1.73 at room temperature and zero stress (pressure). The next step is to propagate this study to include the variation of Ca/Si, hydration level (water to silican ratio, H/Si), temperature and stress. This will enable us to understand the role of each of these chemical and environmental factors in modifying the structure and dynamics of water which in turn will be reflected on the mechanics and chemistry of C-S-H. As a demonstration for the effect of these factors, in Figure 4.1 we show the dependence of the

bulk and shear moduli for the C-S-H model used in this thesis as a function of H/Si. These moduli were calculated using the CSHFF potential by a series of random removal of a single water molecule, relaxation and followed by the calculation of the elastic constants. This is repeated until all water molecules were removed.

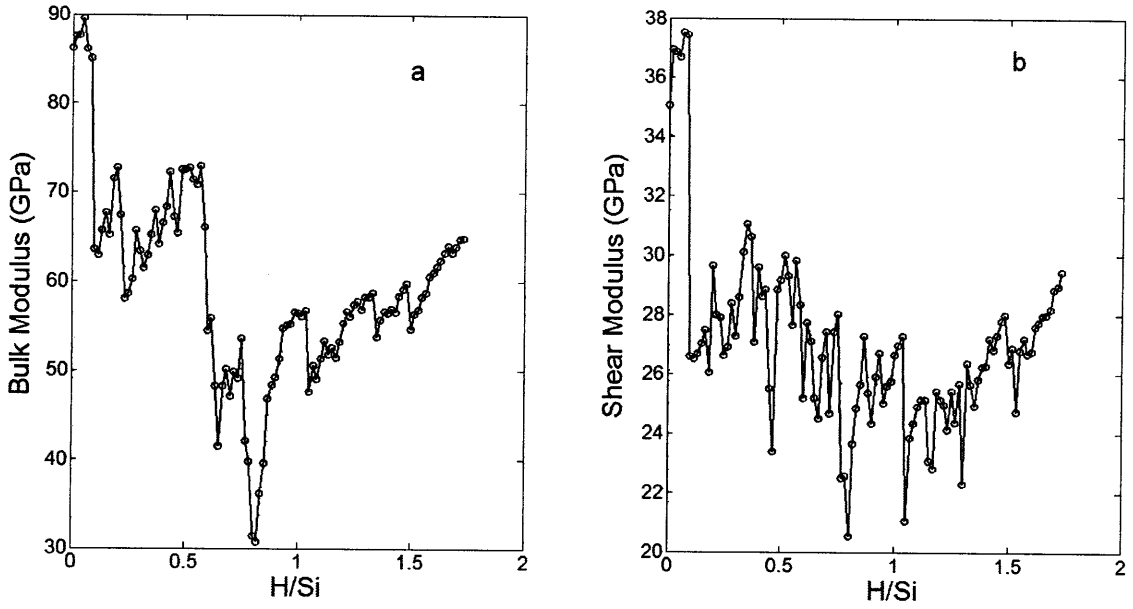

Figure 4.1 Bulk (a) and shear (b) moduli as a function of hydration level, H/Si, for C-S-H at a constant Ca/Si of 1.65.

It is evident that there is a complex non linear dependence of the mechanical properties of C-S-H on the hydration level. In both moduli there is a global minimum at about H/Si $\approx$ 0.8 and another local minimum at H/Si $\approx$ 0.3. We believe that the rough oscillations can be smoothed out by performing finite temperature molecular dynamics at each step of water removal to allow for further relaxations for the atoms.

In addition to this, as we mentioned in Chapter 3, the cationic substitutions in C-S-H changes the equilibrium hydration level and participates in forming a new chemical

environment around the confined water. This interference between the new cations and the water content can be studied by means of grand canonical monte carlo simulations. As we showed in chapter two, the water component in core-shell is not a good description for water, while that of CSHFF is well parameterized. This calls for fitting potentials for cations compatible with CSHFF rather than using core-shell in the study of cationic substitutions in CSH. This also requires more accurate simulation methods, as first principles based approaches, for example in the Density Functional Theory formalism, which can be used later on in fitting these potentials. Finally, experiments that can probe the local structure in C-S-H such as Extended X-ray Absorption Fine Structure (EXAFS), Nuclear Magnetic Resonance (NMR), Neutron scattering and X-ray Diffraction (XRD) are needed to validate these potentials.

Appendix A: Core-Shell and CSHFF Force Fields Parameters

A.1 Core-Shell Force Field Parameters

The core and shell are connected by a harmonic spring with constant k. The potential due to this spring is given by

$$V_i(r_{core-shell}) = \frac{1}{2} k_i r^2_{core-shell} \qquad (A.1)$$

Table A.1 Charges and core-shell spring constants for core-shell

Ion	Core Charge (e)	Shell Charge (e)	Spring Constant k(eV/Å^2)
Calcium (Ca)	2.00000	-	-
Silicon	4.00000	-	-
Layer Oxygen (O)	0.84819	-2. 84819	74.9200
Water Oxygen (Ow)	1.25000	-2.050000	209.4496
Water Hydrogen (Hw)	0.40000	-	-

It should be noted that for anions all non-columbic forces act only on the shells. Also there is no columbic interaction between the core and the shell of the same anion. ***Intra***molecular forces within the water molecule are described by a Morse potential for

the oxygen-hydrogen bond and 50% reduction of the columbic interaction. The form of Morse potential is:

$$V_{ij}(r_{ij}) = D_{ij}(1-e^{-\alpha_{ij}(r_{ij}-r_0)})^2 - D_{ij} \qquad \text{(A.2)}$$

Table A.2 Morse Potential Parameters for Ow-Hw in core-shell.

Ion Pair (ij)	D_{ij} (eV)	α_{ij} (Å^{-1})	r_0 (Å)	Coulomb Subtraction (%)	Cutoff (Å)
Ow-Hw	6.20371	2.2200	0.92376	50	1.20
Hw-Hw	-	-	-	50	1.65

In addition within the water molecule there is a bond-bending term represented by a harmonic form which is:

$$V_{ijk}(r_{ijk}) = \frac{1}{2}k_{ijk}(\theta_{ijk}-\theta_0)^2 \qquad \text{(A.3)}$$

Table A.3 Intramolecular three-body potential for core-shell.

Ions (ijk)	k_{ijk} (eV.rad^2)	θ_0 (rad)	Cutoff (Å)
Hw-Ow-Hw	4.1998	108.69	For Ow-Hw: 1.20 For Hw-Hw: 1.70

The interatomic/intermolecular Buckingham and Lennard Jones parameters are given in Table A.4, A.5 respectively. The analytic form of Buckingham potential is:

$$V_{ij}(r_{ij}) = A_{ij}e^{-r_{ij}/\rho_{ij}} - \frac{C_{ij}}{r_{ij}^6} \qquad \text{(A.4)}$$

Table A.4 Buckingham potential parameters for core-shell.

Ion Pair (ij)	A_{ij} (eV)	ρ_{ij} (Å)	C_{ij} (eV.Å^6)	Cutoff (Å)
Ca-O	1090.40000	0.343700	0.000000	11.5
Ca-Ow	1186.60000	0.297000	0.000000	11.5
Si-O	1283.90700	0.320520	10.66200	11.5
Si-Ow	983.560000	0.320530	10.66158	11.5
O-O	22764.0000	0.149000	27.87900	11.5
O-Ow	22764.0000	0.149000	15.46000	11.5
O-Hw	396.270000	0.250000	0.000000	11.5

The analytic form of Lennard-Jones is:

$$V_{ij}(r_{ij}) = \frac{A_{ij}}{r_{ij}^n} - \frac{B_{ij}}{r_{ij}^m} \qquad \text{(A.5)}$$

Table A.5 Lennard-Jones potential parameters for core-shell

Ion pair (ij)	A_{ij} (eV.Å^n)	B_{ij} (eV.Å^m)	n	m	Cutoff (Å)
Ow-Ow	39344.980	42.150000	12	6	11.5
Ow-Hw	24.000000	6.0000000	9	6	11.5

A harmonic three body term describes the directionality of the covalent bonds of silicon (O-Si-O). The parameters are given in Table A.6.

Table A.6 Interatomic three-body potential for core-shell.

Ions (ijk)	k_{ijk} (eV.rad^2)	θ_0 (rad)	Cutoff (Å)
O-Si-O	2.0972	109.47000	For Si-O: 1.80 For O-O: 3.20

A.2 CSHFF Force Field Parameters

One should note that CSHFF distinguishes between layer oxygen atoms that bridge two silica tetrahedra and the non-bridging ones. Additionally it distinguishes between layer calcium and interlayer calcium. The partial charges are given in table A.7.

Table A.7 Partial charges of CSHFF.

Ion	Partial Charge (e)
Layer Calcium (Ca)	1.435466
Interlayer Calcium (Cw)	1.705529
Silicon (Si)	1.722357
Non-Bridging Layer Oxygen (O)	-1.192286
Bridging Layer Oxygen (Ob)	-1.004228
Water Oxygen (Ow)	-0.8200000
Water Hydrogen (Hw)	0.4100000

There are no columbic interactions within the water molecules. Ow-Hw bond stretching is represented by a harmonic function:

$$V_{ij}(r_{ij}) = \frac{1}{2} k_{ij}(r_{ij} - r_0)^2 \qquad \text{(A.6)}$$

Table A.8 Ow-Hw harmonic bond parameters for CSHFF.

Ions (ij)	k_{ij} (eV.Å^2)	r_0 (Å)	Cutoff (Å)
Ow-Hw	48.05460	1.00000	1.3000

Bond-bending is represented by a harmonic function the parameters of which are in table A.9.

Table A.9 Intramolecular three-body potential for CSHFF.

Ions (ijk)	k_{ijk} (eV.rad^2)	θ_0 (rad)	Cutoff (Å)
Hw-Ow-Hw	3.96914	109.47	For Ow-Hw: 1.30 For Hw-Hw: 1.85

All interatomic/intermolecular interactions are of the Laennard-Jones type (equation A.5). The parameters are given in table A.10. One should note that Ob and O have the same Lennard-Jones parameters but different partial charges.

Table A.10 Lennard-Jones potential parameters for CSHFF.

Ion pair (ij)	A_{ij} (eV.Å^n)	B_{ij} (eV.Å^m)	n	m	Cutoff (Å)
Ow-Ow	27288.2779	27.11991	12	6	11.5
Ca-O/Ob	7193.03500	1.041900	12	6	11.5
Ca-Ow	7248.32200	1.049916	12	6	11.5
Cw-O/Ob	12069.7340	1.748300	12	6	11.5
Cw-Ow	6651.58550	0.834438	12	6	11.5
Si-O/Ob	146.018000	0.119208	12	6	11.5
Si-Ow	121.320800	0.106088	12	6	11.5
O/Ob-O/Ob	37601.3190	90.05472	12	6	11.5
Ow-O/Ob	30487.8730	5.270725	12	6	11.5

Appendix B: Core-Shell Parameters for the Strontium Cation Sr^{2+} and the Hydroxyl Group (OH^-)

In chapter 3 we used the core-shell force field to study the cationic exchange $Sr^{2+} \leftrightarrow Ca^{2+}$ in C-S-H and tobermorite 9 Å. All the core-shell parameters in appendix A applies to this study and in addition we provide here the parameters needed to describe strontium (Sr) and the hydroxyl group oxygen (Oh) and hydrogen (Hh). In this study the real space cutoff for all interatomic interaction is set to 9.7 Å. The following tables summarizes the additional parameters needed to perform this study.

Table B.1 Charges and core-shell spring constants for strontium and the hydroxyl group.

Ion	Core Charge (e)	Shell Charge (e)	Spring Constant k(eV/Å^2)
Strontium (Sr)	2.00000	-	-
Hydroxyl Oxygen (Oh)	0.90000	-2.30000	74.92000
Hydroxyl Hydrogen (Hh)	0.40000	-	-

Table B.2 Morse Potential Parameters for Oh-Hh in core-shell.

Ion Pair (ij)	D_{ij} (eV)	α_{ij} ($Å^{-1}$)	r_0 (Å)	Coulomb Subtraction (%)	Cutoff (Å)
Oh-Hh	7.0525	3.1749	0.9258	0	1.20

Table B.3 Buckingham potential parameters for strontium and the hydroxyl group.

Ion Pair (ij)	A_{ij} (eV)	ρ_{ij} (Å)	C_{ij} (eV.$Å^6$)	Cutoff (Å)
Sr-O	959.10000	0.37210	0.00000	9.7
Sr-Ow	1000.00000	0.322000	0.00000	9.7
Sr-Oh	671.37000	0.37210	0.00000	9.7
Oh-Oh	22764.30000	0.14900	6.97000	9.7
Oh-O	22764.30000	0.14900	13.94	9.7
Hh-Oh	311.97000	0.25000	0.00000	9.7
Ca-Oh	2170.00000	0.29700	0.00000	9.7
Si-Oh	983.56000	0.32053	10.66158	9.7